Ocean Engineering 201 (2020) 107056

Contents lists available at ScienceDirect

Ocean Engineering

journal homepage: www.elsevier.com/locate/oceaneng

An unmanned inland cargo vessel: Design, build, and experiments

Gerben Peeters [a,b,*], Marcus Kotzé [a], Muhammad Raheel Afzal [a], Tim Catoor [a], Senne Van Baelen [a], Patrick Geenen [a], Maarten Vanierschot [a], René Boonen [a], Peter Slaets [a]

[a] KU Leuven, Mechanical Engineering Technology Cluster TC, Campus Group T, Andreas Vesaliusstraat 13, 3000, Leuven, Belgium
[b] Research Foundation - Flanders (FWO), Egmontstraat 5, 1000, Brussel, Belgium

ARTICLE INFO

Keywords:
Autonomous
Unmanned
Inland
Vessel
Experiment
Build

ABSTRACT

Although road-based freight transport has large external costs, it currently dominates the hinterland cargo transport sector in Europe. An increase of the automation levels of inland cargo vessels could advance their competitiveness, hence unlocking more sustainable inland cargo transport. Moreover, these improvements could pave the way for a potential future paradigm shift towards unmanned inland cargo vessels. Therefore, this study investigates the design of an experimental platform in order to study the feasibility and current or future limitations of unmanned inland cargo vessels. To explore this design, the following three questions were handled: (i) How to design an industrially relevant research vessel?, (ii) How can an unmanned inland cargo vessel interact with or perceive its environment?, and (iii) How to control an unmanned or autonomous inland cargo vessel? The answers to these design questions delivered the blueprint to construct a first prototype of an unmanned inland cargo vessel. This prototype performed a set of outdoor experiments to verify and validate the made design choices. The successful execution of these experiments demonstrates that this vessel can serve as an experimental platform for further technological research regarding more automated or unmanned inland cargo vessels and provide fruitful insights for other research domains.

1. Introduction

Currently, road-based freight transport dominates the European hinterland transport sector, enveloping roughly 75% of the cargo flow expressed in tonnes*km (tkm), and it has been doing so for the last 25 years (European Commission, 2019). Given the fact that road-based freight transport currently suffers from congestion, together with the increased restrictions on its emissions, a solution needs to be found to sustainably cope with the projected rise in cargo flow in the upcoming decades. For example, the Belgian Federal Planning Bureau estimates a total cargo growth of +27% (tonnes) in the period between 2015 and 2040 caused by a 5% rise of national transport and a 39% rise of international transport over Belgian territory (under the assumption of unchanged policies). Similarly, they estimate an increase of +32% (tkm) of goods transported over inland waterways (Laine et al., 2019).

These projected cargo growths show both the magnitude and internationality of the transport problem at hand. It is for this reason that the European Commission has set the ambitious goal to push 30% (tkm) of road freight transport, longer than 300 km, to rail and water-borne transport between 2011 and 2030, and likewise 50% (tkm) by 2050 (Kallas, 2011). This envisaged transformation of the multi-modal transport network leverages the knowledge that the average external costs (accidents, air pollution, climate, noise, and congestion) for inland waterway transport are significantly lower than for road transport (Al Enezy et al., 2017; van Essen et al., 2011). To illustrate this cost difference, note that the average total cost, hence including external costs, for inland waterway transport equalled an estimated 3.9 EURcent/tkm in Europe in 2016, which was almost half of the similar road costs which amounted to 6.6 EURcent/tkm (van Essen, 2018), where both numbers additionally include well-to-tank and habitat damage costs.

Although inland waterway transport seems to be a more sustainable alternative to road transport, it currently suffers from an outflow of small vessels of the European Class type I and II (often referred to as CEMT I and II, where CEMT is a French abbreviation for *Conférence Européenne des Ministres de Transport* (CEMT, 1992)). Some of the main reasons for this recorded outflow are: (i) a lack of technological improvements, (ii) a reduction of new young skippers, and (iii) high crew costs, which can rise up to 60% of the transportation cost (Sys and Vanelslander, 2011). This diminishing fleet of small vessels could cause a discrepancy with the philosophy of the European Commission to shift cargo loads to the inland waterway transport. Consequently, to

* Corresponding author. KU Leuven, Mechanical Engineering Technology Cluster TC, Campus Group T, Andreas Vesaliusstraat 13, 3000, Leuven, Belgium.
E-mail addresses: gerben.peeters@kuleuven.be (G. Peeters), peter.slaets@kuleuven.be (P. Slaets).

https://doi.org/10.1016/j.oceaneng.2020.107056
Received 22 August 2019; Received in revised form 31 January 2020; Accepted 1 February 2020
Available online 5 March 2020

Nomenclature

Sensor and Communication Abbreviations

3G/4G	third/fourth Generation
BMS	Battery Management System
CAN	Controller Area Network
EKF	Extended Kalman Filter
ESTOP	Emergency Stop
GNSS	Global Navigation Satellite System
I–PC	Industrial Computer
IMU	Inertial Measurements Unit
IP	Internet Protocol
IP-rating	Ingress Protection rating
LIDAR	Laser Imaging Detection And Ranging
Mbps	Megabit per second
PLC	Programmable Logic Controller
POE	Power Over Ethernet
PWM	Pulse-Width Modulation
R–PC	Rugged Laptop/Computer
RADAR	RAdio Detection And Ranging
RC	Remote Controller
RS232	Recommended Standard 232
RTK	Real Time Kinematic
SSI	Synchronous Serial Interface
TCP	Transmission Control Protocol
UDP	User Datagram Protocol
WLAN	Wireless Local Area Network

General Abbreviations

CEMT	European vessel types based on: Conférence Européenne des Ministres de Transport
AIS	Automatic Identification System
ASV	Autonomous Surface Vehicle/Vessel
EFRO	European Fund for Regional Development
GNC	Guidance, Navigation, Control
H2H	Hull-to-Hull
IMO	International Maritime Organisation
MOOS	Mission Oriented Operation Suite
MOOS-IvP	MOOS Interval Programming
MOOSApps	MOOS Applications
MOOSDB	MOOS DataBase
MUNIN	Maritime Unmanned Navigation through Intelligence in Networks
PID	Proportional, Integral, Differential
RIS	River Identification System
ROV	Remotely Operated Vehicle/Vessel
rpm	revolutions per minute
SP-CEMT	Self Propelled CEMT vessel
TEN-T	Trans-European Transport Network
tkm	tonne-kilometre
USV	Unmanned Surface Vehicle/Vessel

Symbols

θ_i^b	Internal control angle bow thruster [°]
θ_i^s	Internal control angle stern thruster [°]
θ_o^b	Output angle thrust force bow [°]
θ_o^s	Output angle thrust force stern [°]
B_A	Blade area ratio propeller [-]
D^b	Diameter bow propeller [mm]
D^s	Diameter stern propeller [mm]
K_i	Integral gain factor $[1/s]$
K_p	Proportional gain factor [-]
n^b	Propeller speed bow [rpm]
n^s	Propeller speed stern [rpm]
P_D	Pitch-Diameter ratio propeller [-]
T^b	Thrust force bow [N]
T^s	Thrust force stern [N]
T_x^s	Decomposed thrust force stern on x-axis [N]
T_y^s	Decomposed thrust force stern on y-axis [N]
x, y, z	Coordinates in the body-fixed frame [m]

accomplish the conceptualised modal-shift, this projected gap between the increasing need of inland waterway transport and the acknowledged outflow of CEMT I-II vessels might need to be filled.

The authors believe that an increase in the automation levels of inland cargo vessels could be part of the solution to increase the sustainability of the multi-modal transport network of the European hinterland. Furthermore, this improvement could unlock the possibility of unmanned inland cargo vessels, which could induce a paradigm shift in this transport sector. To be able to study this possibility of unmanned inland cargo vessels, the authors think that an industrially-relevant, experimental test platform will generate vital information. Therefore, they explored the question of: How to design an experimental platform to study the feasibility and current or future limitations of unmanned inland cargo vessels? Evidently, not all research challenges can be known up front, nor can all possible solutions be properly accommodated on one research vessel. Therefore, this paper focusses on three key technological design aspects: industrial relevance, vessel-environment interactions, and the motion control of the vessel. Note that some of the research results for an unmanned vessel can be transferred to its manned counterparts, in order to increase their automation level.

Be aware that the technological achievability of this industrial platform alone cannot judge the economical feasibility of unmanned inland cargo vessels in general. Nevertheless, the authors believe that this platform will form an indispensable piece in the potential future automation puzzle. For example, in a recent study regarding potential business cases for more automated inland waterway transport, Verberght and van Hassel (2019) state that defining the automated or unmanned vessel remains quite challenging and open for debate which impacts the accuracy of the cost analyses. Hence, the experimental results of this study could be used to investigate the economical feasibility on a higher level of resolution, and the same principle could hold for different research domains looking into automated or unmanned inland shipping.

The remainder of this paper continues as follows: section 2 outlines the current research field regarding Unmanned or Autonomous Surface Vessels (USVs or ASVs), identifies some of the key technological challenges for unmanned inland cargo vessels, and details the three aforementioned key design aspects of this paper, which the three following sections will discuss. Subsequently, section 3 handles the industrial relevance of the research vessel, section 4 discusses its interactions with the environment, and section 5 explains the chosen motion control implementation. Afterwards, section 6 discusses the first experiments conducted with the constructed vessel. Finally, section 7 concludes the aforementioned topics and uncovers some of the potential technological future research areas for unmanned inland cargo vessels.

2. USV research field and challenges

2.1. USV research field

The advancements in platforms, sensors, onboard computing power, and communication systems have reached critical maturity levels over

the last two decades (Benjamin, 2016), and additional improvements occurred for the implementation of Guidance, Navigation, and Control (GNC) subsystems (Fossen, 1994; Fossen, 2002; Do and Pan, 2009; Fossen, 2011), which help to form the intelligent backbone of a USV. The combination of these developments gradually unlocks more potential for semi- or fully-autonomous surface vehicles, which has resulted in the growth of five main USV categories: (i) scientific research, (ii) environmental missions, (iii) ocean resource exploration, (iv) military use, and (v) other applications, as defined by Liu et al. (2016). They also noted the scarcity of USVs in the commercial markets, which could be explained by their continuous competition with their manned analogues or with other robotic platforms (Savitz et al., 2013). Concerning the more cargo-oriented USV research, Moreira and Guedes Soares (2011) conducted research on a scale model sea-going vessel to perform manoeuvring tests autonomously without a specific focus on the industrial use or design of the vessel itself. Furthermore, within the concept study of the recent ReVolt project, which aims at safe, efficient, and environment friendly short sea shipping (Midjas, 2018), a scale model has been built with no specific focus on the industrial robustness of the model. It is also noteworthy that one of the conclusions of the MUNIN (Maritime Unmanned Navigation through Intelligence in Networks) project (MUNIN, 2016) was that inland cargo vessels might be plausible first movers for unmanned cargo shipping, if suitable business models could be found. This idea originates from the presumed lower legal and technological complexity of inland cargo shipping compared to deep sea cargo shipping (Rødseth, 2015).

2.2. Technological challenges for inland USVs

Although the technological complexity might be assumed to be lower at first glance, the overall challenges for unmanned inland shipping are not trivial. For instance, inland ships suffer from a spatially more restricted complex navigational environment, and have no help of tugs to manoeuvre (Liu et al., 2015). Moreover, the horizontal and vertical confinements of the waterway have a significant influence on the hydrodynamic behaviour of a vessel (Pompée, 2015) and bank effects occur when sailing close to a quay or other infrastructures (Lataire et al., 2018). The identification of these hydrodynamic effects is paramount for advanced GNC modules, but not available for smaller inland vessels (Liu et al., 2017). Furthermore the usability of these GNC modules for inland navigation needs to be investigated and further developments might be necessary. Likewise, the perception of the environment of an inland vessel needs to be explored and crucial information will need to be shared over, and fetched from, the Automatic Identification System (AIS) and the River Information System (RIS) (Vallant and Hofmann-Wellenhof, 2008).

2.3. Technological design aspects for inland USVs

In order to be able to study these inland-specific technological challenges for unmanned inland cargo vessels, an industrially relevant research vessel has to be designed and constructed, which envelops the aim of this study. This aim can be tailored down into the following three research questions, answered by the following three sections:

(i) How to make a research platform for an unmanned inland cargo vessel industrially relevant?
(ii) How can an unmanned inland cargo vessel interact with or perceive its environment?
(iii) How to control an unmanned inland cargo vessel?

3. Industrial relevance

When designing an experimental platform that has the ambition to explore unmanned inland cargo shipping, its design needs to have a certain level of industrial relevance in order for it to generate useful data or insights. Four main design choices that resulted in an increase of industrial relevance were made: (i) the vessel type and size, (ii) the actuation system, (iii) the component selection, and (iv) the modular design in both hardware and software.

3.1. Vessel type and size

Two industrial developments for inland vessels drove the decision of the vessel type and size, discussed by section 3.1.3. On the one hand, the European Watertruck$^+$ project introduces a fresh batch of inland vessels, reviewed by section 3.1.1, and, on the other hand, a growing research and industrial interest for urban cargo vessels has been triggered in Europe, explained by section 3.1.2.

3.1.1. Industrial Watertruck$^+$ project

An attempt to bridge the gap between the growth of inland cargo transport and the outflow of small inland vessels has been made by the European Watertruck$^+$ project (European Commission, 2018b), which is situated in the broader Trans-European Transport Network (TEN-T (European Commission, 2018a)) framework. This Watertruck$^+$ project envisages an increased flexibility in waterborne transport by introducing a modular fleet of both barges and push boats which can easily be coupled or decoupled, in a truck or train-like fashion. Not only does this modularity provide the on demand configuration of ship fleets, it also decouples sailing and transshipment time, further reducing the crew costs on board. In its first phase, the Watertruck+ project will introduce 31 new barges and push boats (12 unpropelled barges, 16 self-propelled barges and 3 push boats) of CEMT type I-II. The final deliverable aims to expand this fleet to 500 vessels in the CEMT range I to IV (European Commission, 2018b).

3.1.2. Vessels for urban transport

Evidently, a smaller vessel can penetrate deeper in the European hinterland and could even enter certain urban areas. Nevertheless, urban waterborne freight transport remains complex to organise and needs further research. However, smaller-scale cargo transport has been shown to be a workable alternative in urban areas in several European cities (Janjevic and Ndiaye, 2014). For example, in 1996, the city of Utrecht, the Netherlands, introduced a boat of length 18.80 m, beam of 4.26 m, and a maximum draft of 1.10 m, to cope with the increasingly difficult road-based urban city logistics due to their narrow road ways, and a second boat was introduced in 2010 with an electric power supply (Maes et al., 2012). Additionally, Caris et al. (2014) suggested that further research could support an increased integration of inland waterway transport into urban distribution networks, which could also help a further integration of inland waterway transport in the inter-modal supply chain.

3.1.3. Experimental platform geometry

Given the above-mentioned fresh batch of CEMT I-II vessels, on the one hand, and the growing research interest in urban freight transport over inland waterways, on the other hand, the experimental platform geometry design was chosen to be a scale model of a Self-Propelled CEMT-I (SP-CEMT I) Watertruck$^+$ vessel. By taking a scale factor of 8, the vessel can serve as a research platform to both study the SP-CEMT I fleet, and to investigate some of the possibilities of urban waterway logistics. Table 1 lists the geometrical similarity between the SP-CEMT I and its scale model, named the *Cogge*,[1] and Fig. 1 shows this geometry of the SP-CEMT I, or Cogge, together with its body-fixed reference frame where the x-axis points to the bow, y-axis to starboard, and the z-axis downwards. Additionally, Fig. 2 (a) depicts a convoy of four CEMT I barges being pushed by a manned push boat, and (b) shows the KU

[1] As a tribute to Karel Lodewijk Cogge who helped flooding the plains of the Yser during the first World War to keep the German troops at a distance.

Table 1
Geometry SP-CEMT I and Cogge.

	SP-CEMT I	Cogge	
Scale	1	8^{-1}	-
Length	38.50	4.81	m
Breadth	5.05	0.63	m
$Draft_{empty}$	0.60	0.075	m
$Draft_{full}$	2.80	0.35	m
Block coefficient	0.95	0.95	-
$mass_{empty}$	110 000	215	kg
$cargo_{maxixmum}$	395 000	771	kg
$mass_{full,maximum}$	505 000	985	kg

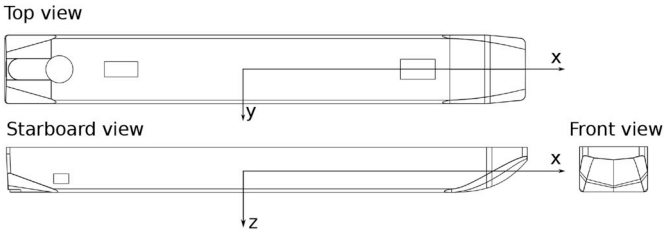

Fig. 1. Bare hull of a Watertruck+ push barge type CEMT I. The visible holes are to fully integrate the actuation systems.

Leuven scale model of such a self-propelled barge, deployed as a USV.

It is impossible to physically board the Cogge, hence making it a USV by raw definition. Nevertheless, it would be possible to board and steer its real-size counterpart. This discrepancy in operational modes may lead to some confusion between *unmanned* and *autonomous*, as both adjectives are not mutually exclusive in this context. Similarly, the literature regarding surface vehicles often discusses both ASVs and USVs interchangeably (Bertram, 2008; Manley, 2008; Campbell et al., 2012; Liu et al., 2016). Moreover, the exact meaning of *autonomous* is often vaguely described as it inherently entails different levels which may be context dependent. Rødseth and Nordahl (2018) proposed definitions to further clarify the surface-vehicle nomenclature taking into account both ship specific situations (e.g. having a temporarily unmanned bridge on a manned vessel) and different levels of autonomy. Fig. 3 lists these autonomy levels, ranging from direct (physical) control by the crew to fully autonomous (i.e. unmanned without supervision) together with their interactions with the vessels in this study. As visualised, the real size SP-CEMT I can be both an ASV, when it has crew on board, and a USV, when there is none. Moreover, both vessels will be remotely steerable, also making them Remotely Operated Vehicles (ROVs).

3.2. Actuation system

Two key aspects motivated the actuation system selection, with a focus on industrial relevance: (i) the system should be used by existing or future inland cargo vessels, and (ii) if possible, the system should be generic. Both criteria were met by scaling down the propulsion system of the Watertruck^{+} SP-CEMT I barges. These barges have a novel actuation configuration enveloping a 360-degrees-rotatable steering-grid thruster in the bow in conjunction with a 360-degrees-rotatable 4-channel thruster in the stern. Firstly, this over-actuated propulsion system is currently used by the real-scale vessels and it unlocks the possibility to perform more complex manoeuvres and subsequent advanced motion control philosophies. And secondly, such an over-actuated system can be used to mimic an under-actuated system by digitally disabling or limiting certain control parameters, making it a modular and generic actuation system. Peeters et al. (2019) discuss this novel actuation combination nested inside the Cogge, and this section will summarise the most relevant parts from their study in order to understand the full vessel design. The propulsion system is completely integrated in the hull, i.e. no parts protrude the vessel. This nested configuration generates lower manoeuvring limitations in the often spatially restricted inland waterways. Fig. 4 shows a transparent view of the vessel with its bow and stern thruster, which are discussed in section 3.2.1 and section 3.2.2 respectively.

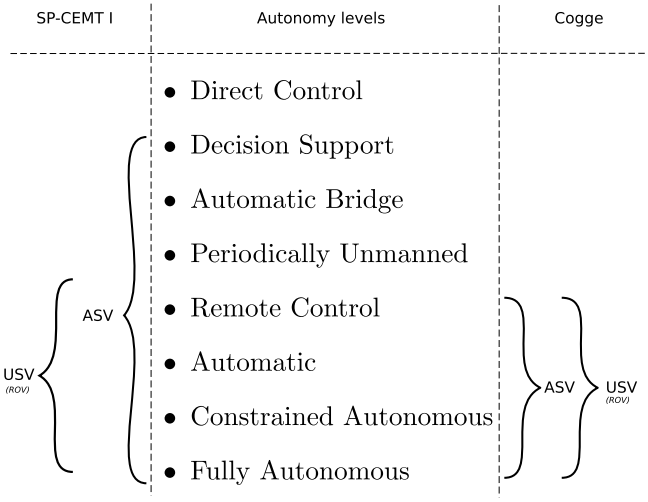

Fig. 3. Surface vehicle nomenclature for the CEMT I self-propelled barge and its scale model at different autonomy levels, based on Rødseth and Nordahl (2018).

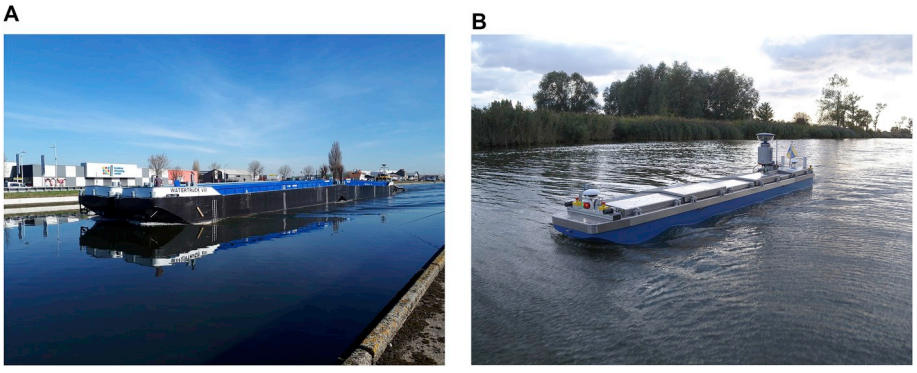

Fig. 2. (a) Watertruck+ convoy: consisting of four CEMT I barges pushed by one push boat (slightly visible on the right hand sight), and (b) the KU Leuven scale model.

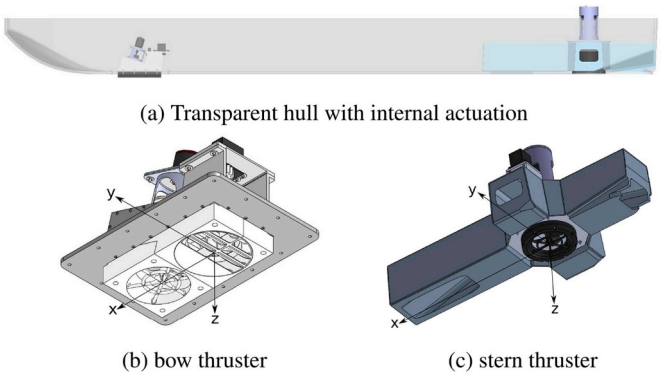

Fig. 4. Actuation System nested inside the hull (a), bow thruster (b), and stern thruster (c), adapted from (Peeters et al., 2019).

3.2.1. Bow thruster

The bow thruster has a Kaplan Series propeller without nozzle with a diameter of $D^b = 100\,mm$, a blade area ratio of $B_A = 0.65$, and a pitch-diameter ratio of $P_D = 0.95$. This horizontally oriented propeller (i.e. its rotational axis stands (almost) perpendicular to the calm water plane) draws in water from underneath the hull, and afterwards this water flow exits the actuator according to the orientation of the internal steering grid angle, θ_i^b. An abstract representation of this working principle is show by Fig. 5, for $\theta_i^b = 0°$ and 90°. For this bow thruster, it is assumed that θ_i^b and the output angle, θ_o^b, of its resulting thrust force, T^b, always align (i.e., $\theta_i^b = \theta_o^b$), hence the chosen angle convention immediately gives the orientation of T^b as the water flow exits the actuator in the opposite direction.

Fig. 6 shows the measured thrust forces, linearly extrapolated, at different rotational speeds of its propeller, n^b, and different θ_i^b. These data were measured without an enveloping ship hull and without any ship velocity, hence external hull losses and wake influences are not incorporated. A significant loss in T^b emerges at $\theta_i^b = \theta_o^b \in [150°, 180°]$ which might be explained by the possible occurrence of a closed loop system of circulating water as the outlet angle, θ_o^b, of the exiting water stream is oriented towards the propeller.

3.2.2. Stern thruster

The stern actuation operates with a slightly larger, but geometrically similar, propeller of diameter $D^s = 150\,mm$. Fig. 7 demonstrates the basic working principle of this actuation system: half a sphere, with an

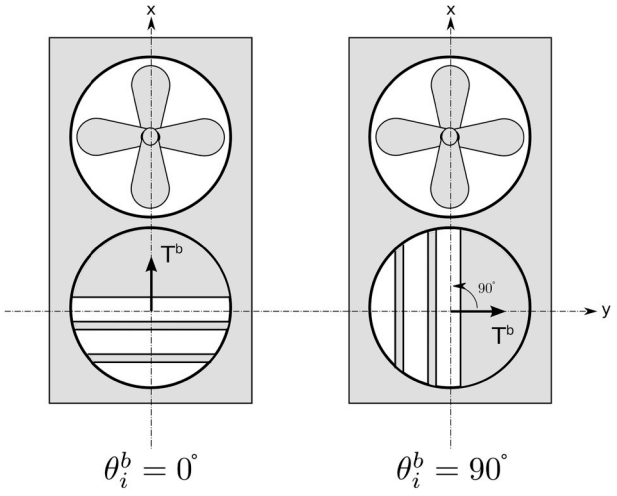

Fig. 5. Top view of the bottom section of bow thruster for $\theta_i^b = 0°$ and 90°, adapted from (Peeters et al., 2019).

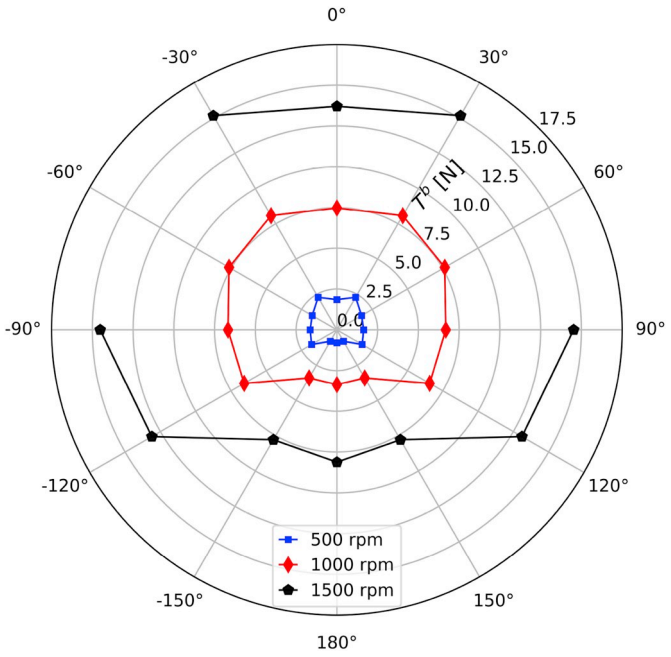

Fig. 6. Experimental results thrust force bow, T^b, at different actuator angles, θ_i^b, and propeller speeds, n^b. Note that there was no measurement for $\theta^b = 60°$ at $n^s = 1500$ rpm, and that the plot assumes symmetry over the x-axis.

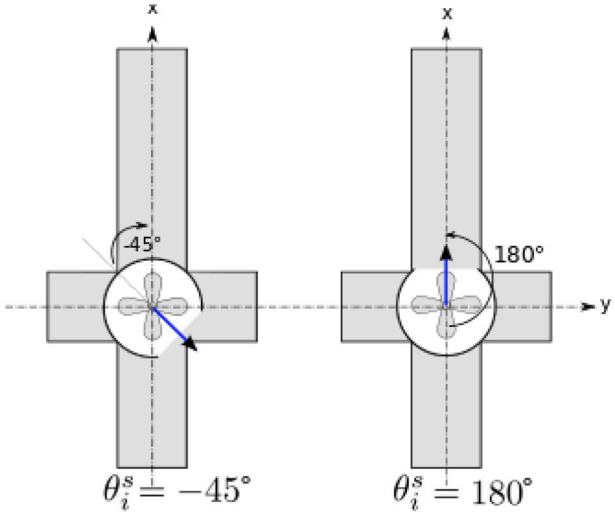

Fig. 7. Top view of the bottom plane of the stern thruster for internal actuation angle $\theta_i^s = -45°$ (left) and $= 180 = -180°$ (right), where the blue arrow denotes a virtual water outflow if θ_i^s would equal θ_o^s, adapted from (Peeters et al., 2019). (For interpretation of the references to color in this figure legend, the reader is referred to the Web version of this article).

opening of approximately 85°, stands above the propeller and can be controlled by its internal angle, θ_i^s in order to orient the outflow of water through one of the four channels, or through a superposition of two.

Experimental data were fetched with the stern thruster nested inside half a ship hull (transversal cut at midship) at zero velocity in a towing tank. Hence, the main external hull losses were incorporated and no wake influences were present. Fig. 8 depicts the arising thrust forces at different propeller speeds, n^s, and different θ_i^s, which were measured on both the longitudinal axis, T_x^s, and the transversal axis, T_y^s, of the actuation system. The data indicate two main non-linearities: one at $\theta_i^s \in [60°, 120°]$ for T_x^s and the other at $\theta_i^s \in [150°, 180°]$ for T_x^y. The resulting stern thrust force, T^s, and its output angle, θ_o^s, can be calculated

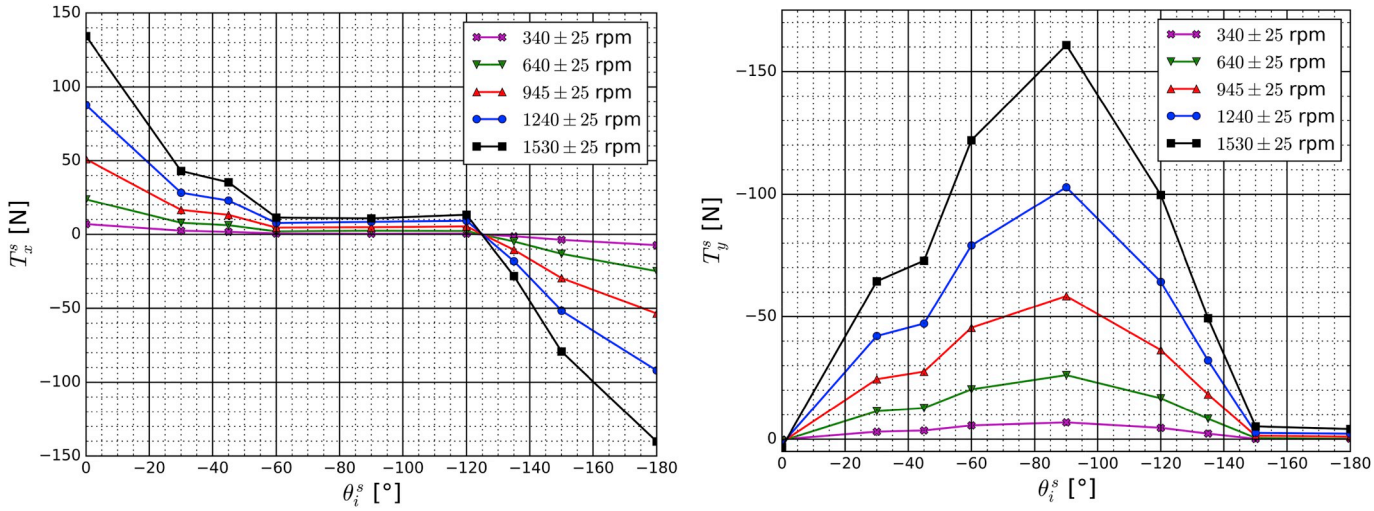

Fig. 8. Orthogonally decomposed experimental results from the thrust forces of the stern thruster T^s, adapted from Peeters et al. (2019).

as follows:

$$T^s\left(n^s,\theta_i^s\right)=\sqrt{T_x^s(n^s,\theta_i^s)^2+T_y^s(n^s,\theta_i^s)^2},\quad \theta_o^s=\arctan\left(\frac{T_y^s}{T_x^s}\right) \tag{1}$$

The mapping of the resulting θ_o^s on the requested θ_i^s, as shown by Fig. 9, shows that the abovementioned non-linearities have a large effect on the orientation of T^s as these constant thrust zones reappear at the same angle intervals [60°, 120°] and [150°, 180°]. The exact cause of this non-linearity is hard to uncover but some of the likely contributors seem to be: (i) the difference in length and shape of the four channels, (ii) the potentially remaining angular velocity of the water inside the system, and (iii) the internal reflections of the water stream, in the xy-plane, when $\theta_i^s \neq 0°, 90°, 180°$, or $-90°$.

3.3. Component selection

The selection of robust, industrial, and marine-grade components (where possible) further increased the industrial relevance of the vessel. Table 2 reflects these design choices by listing the main components of the Cogge and its associated shoreside infrastructure, and Fig. 10 shows their location on the Cogge. As can be seen, both the control hardware (programmable logic controller, industrial computer, industrial router, …) and the sensors have an industrial level that could be transferred to a real-size vessel. In this manner, the Cogge can experiment with a

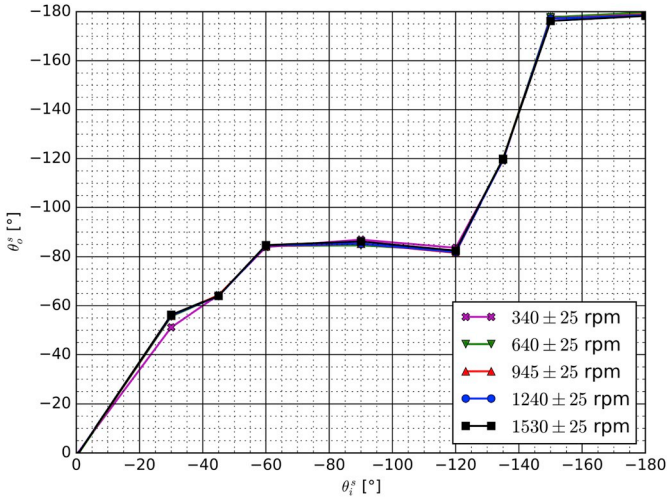

Fig. 9. Mapping of θ_o^s and θ_i^s. Adapted from Peeters et al. (2019).

Table 2
List of components, their description, and their abbreviations.

Nr.	Description	Abbreviation/ Name	Type
1	Programmable logic controller	PLC	Wago PFC200 750-8207
2	Industrial computer	I-PC	MC-7200-MP-T
3	Rugged shoreside laptop	R–PC	Dell Latitude Rugged 7204
4	Remote controller	RC	IK3 Danfoss (two joysticks)
5	Industrial Router	Quartz	Quartz-LTE
6	Power over Ethernet switch	POE switch	5-port 1000 Base-T Industrial Eco Switch
7	Navigational GNSS sensor	GNSS	AsteRx-U MARINE
8	Inertial measurements unit	IMU	EKINOX2-E-G4A3
9	Laser scanner	LIDAR	OPAL-1000
10	Stereo cameras	Cameras	UI-5280FA-C-HQ, from IDS Built by Vision++
11	Motor bow thruster	Bow motor	Turnigy RotoMAx 150 cc
12	Motor drive bow thruster	Bow motor drive	Roboteq MBL1660A
13	Bow angle integrated stepper	Bow angle quickstep	JVL MIS234S
14	Motor stern thruster	Stern motor	Turnigy Aerodrive SK3-6364-245 KV
15	Motor drive stern thruster	Stern motor drive	Roboteq MBL1660A
16	Stepper motor stern angle	Stern angle stepper	34SM095
17	Motor drive stern stepper angle	Stern angle stepper drive	MSD-50-5.6
18	Encoder stern angle	Stern encoder	RSC-2832-212-441-436
19	3 bilge pumps	Bilge pumps	Rule Bilge pump 800
20	4 emergency stops	ESTOP	Twist to reset 40 mm Mushroom
21	Stern light	Stern light	LED white 12–24 V
22	Directional lights bow	Port/Starboard light	Allpa LED 2 colors 8–30 V
23	Battery 24 V	24 V DC	24 V, 5000 Wh, Navex
24	Battery 12 V	12 V DC	12 V, 2500 Wh, Navex
25	Battery monitoring system	BMS	Mastervolt – Amperian interface

configuration that could be used by real-size inland vessels during their normal operations.

The power supply to feed all these components consists of two batteries. Although the lower energy density of the current battery technology introduces a significant weight and price penalty compared to a

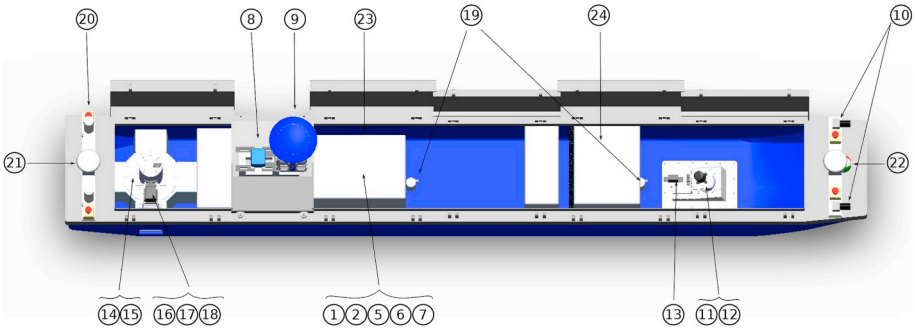

Fig. 10. Top view 3-dimensional drawing of the Cogge (slightly tilted), stern on the left and bow on the right. The vessel lights, parts nr. 21 and 22 are mounted underneath the visible white GNSS mushroom antennas.

fuel-based system, it was judged to be more convenient to use for the scale model for three main reasons: (i) less noise and vibrations, (ii) no local emissions near researchers, and (iii) the vessel can be charged by a 220–230 V AC power supply in a few hours. A detailed implementation of this charge system can be found in the Appendix. This fully electric drive train causes a difference between the Cogge and the first batch of SP-CEMT I vessels which can use a hybrid system enveloping both batteries and diesel generators to power their electrical engines. This hybrid system aligns with the growing research field looking into hybrid propulsion systems for vessels (Kalikatzarakis et al., 2018) which might cause a change in the default drive train layouts of future vessels.

3.4. Modular hardware and software

The fourth and final industrially-relevant design aspect was achieved by focussing on a modular system design on both the hardware and software level. By doing so, the final construction of the Cogge remains flexible as different hardware components could be tried out in the future, or added to the current design, and different autonomy software could control the vessel, or different motion control philosophies could run in the current autonomy software.

3.4.1. Modular hardware

Three main subsystems form the overarching hardware and subsequent communication architecture: an actuation control subsystem, a sensor and autonomy subsystem, and a shoreside subsystem. Fig. 11 illustrates their vital inter- and intra-communication links.

The actuation control subsystem houses a second level of modularity induced by the nested PLC topology. This PLC controls the lowest level desired actuation system states, i.e. n^b, n^s, θ_i^b, and θ_i^s, and these states can be communicated to the PLC via currently three devices: (i) the remote control over a radio link, (ii) a web-interface over mobile or wireless internet, and (iii) the onboard industrial computer over a Modbus TCP/IP connection. After the reception of these desired system states, the PLC will communicate these states to their appropriate actuation system drivers which will then, using their internal control loops, drive these states to their desired value. In this fashion: two motor drives control n^b and n^s, a stepper motor with an integrated encoder controls θ_i^b, whereas the stepper motor for θ_i^s and its complementary encoder are currently two separated entities, but they will be replaced by one entity in the future which will be added on the CAN fieldbus. Furthermore, this cascaded configuration makes the PLC the heart of the vessel and

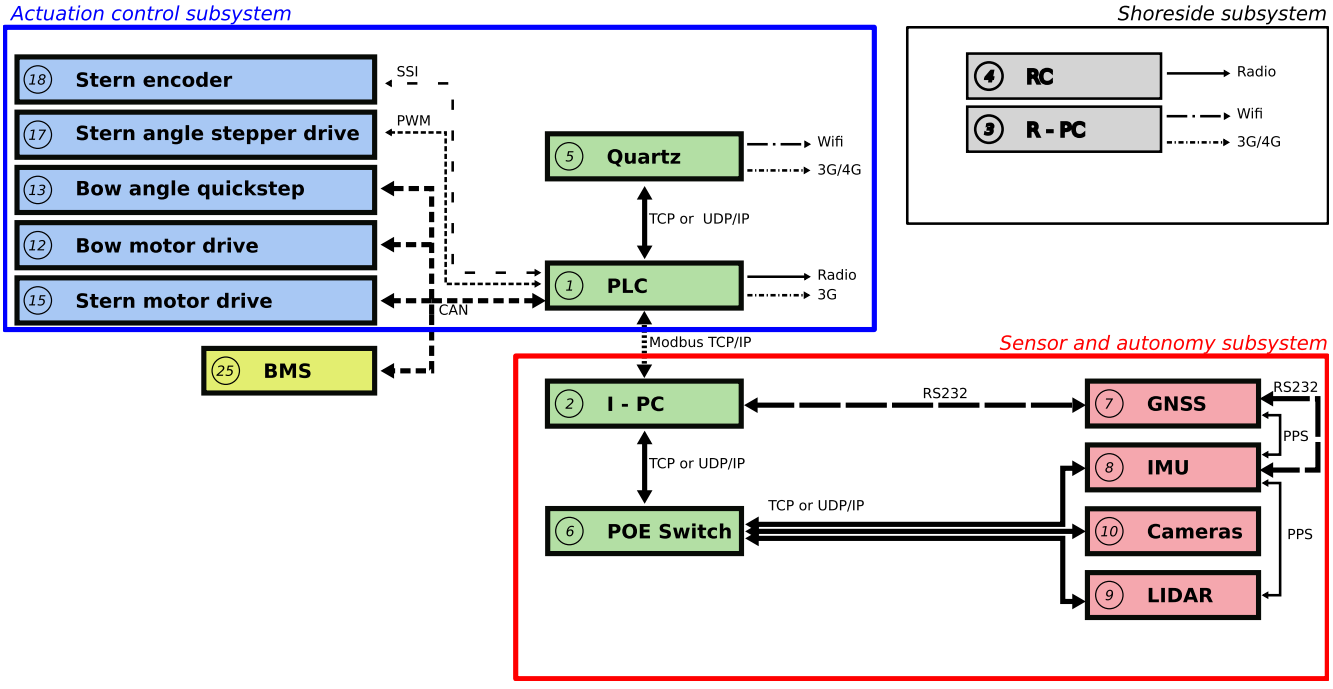

Fig. 11. Inter- and intra-communication links of the different hardware subsystems, where the following background color code was used: blue for actuation components, red for sensors, grey for shore-side parts, green for the main onboard communication and computing devices, and yellow for the battery system. (For interpretation of the references to color in this figure legend, the reader is referred to the Web version of this article).

exploits its industrial robustness to control the desired system states. This lay-out achieves an increased level of operational redundancy, which is paramount for industrial applications.

The industrial computer forms the core of the sensor and autonomy subsystem. On the one hand, it receives the sensor information (currently GNSS (Global Navigation Satellite System), IMU (Inertial Measurements Unit), Camera, and LIDAR (Laser Imaging Detection and Ranging), and on the other hand it runs the autonomy software (see section 3.4.2), which can use this sensor information to provide the motion control (see section 5) of the Cogge.

The third and final hardware subsystem accumulates all the shoreside infrastructure, which currently consists of the rugged shoreside laptop, and a remote control. The latter provides the possibility for manual control of the vessel, as it is not possible to board the Cogge, whereas the shoreside laptop provides further visual feedback as it can communicate with the onboard processes. The remote control has two physical joysticks to steer the propeller speeds and control angles of the actuation systems, note that these variables can also be set via a web-interface.

3.4.2. Modular software

An autonomy system nested on the I-PC can also control the vessel instead of a human. Modularity and genericness formed two of the key design choices for the selection of this autonomy software. Therefore an open-source cross-platform software suite was chosen named Mission Oriented Operations Suite (MOOS) (Newman, 2005). This MOOS software provides internal asynchronous publish-subscribe communication between MOOS Applications (MOOSApps), which are small modular software entities (C++), via its DataBase (MOOSDB), and can be used for robotic research in general. Encompassing this MOOS-core, Benjamin et al. (2010) wrote a marine-oriented expansion of this software called MOOS Interval Programming, or MOOS-IvP, which takes advantage of the backseat driver paradigm. This backseat paradigm separates the vehicle navigation and control parts from its autonomy system, making the latter research platform independent. This paradigm implementation further increases the modularity and genericness of the control architecture of the Cogge. Furthermore, on the Cogge, the control architecture consists of three cascaded levels coined high, middle, and low level control, which will be discussed in section 5.

4. Environment interactions

An unmanned or automated vessel needs to perceive and interact with its environment in order to navigate. For the purpose of understanding the environmental settings in which the vessel could sail, the authors made the following arbitrary differentiation based on the present obstacles, where obstacles envelop both the waterway infrastructure (such as bridges, locks, quays, waterway cross-section, …), and other vessels: (I) static known obstacles, (II) static unknown obstacles, (III) dynamic known obstacles, and (IV) dynamic unknown obstacles. Here, the adjective *known* means that information (geometry, position, orientation, potential velocity, …) about the object is available, and the opposite holds for the unknown objects. From the moment that one object in the environment is unknown or dynamic, the environment changes to its associated description. It is readily understood that other environmental differentiations could be made, depending on the preferred level of analysis of the researcher.

These four environments seem to demand different sensor capabilities from the vessel on the one hand, and different risk and safety analyses on the other hand. The former should provide the vessel with both navigational information and perception of its ambient environment, respectively discussed in the subsequent sections 4.1 and 4.2. An in-depth discussion of the latter falls out of the scope of this study, nevertheless, observe that there is movement in this research area. For example, Megumi and Susumu (2019) investigated how to introduce autonomous maritime vessels into the existing International Maritime Organisation (IMO) regulations, and (Thieme et al., 2018) investigated the applicability of 64 existing ship risk models for ship-ship collisions, ship-structure collisions, and groundings for autonomous marine vessels. The latter concluded that for a more detailed system evaluation more information regarding the USV concept needs to be known. Valdez Banda et al. (2019) complementarily noted the major challenge of ensuring the safety of a USV in its operational context given the limited experience with functioning USVs. Therefore, they analysed the safety hazards for two ferries in their current operational modes and in their potential autonomous deployments. Finally, the inclusion of a shore control centre, to monitor or remotely steer a USV, further complicates the risk analyses by introducing human-system interactions. Unfortunately, here too, a deficiency in the amount of research considering such human-system interactions and potential human failures was noted by Abilio Ramos et al. (2019). Consequently, they studied how humans in a shore control centre could form a key component for successful collision avoidance by uncovering their potential tasks and the impact of the possible human failures to perform these.

Considering that a common denominator over these recent USV risks analyses seems to be the scarcity of operational USV concepts, the developments in this study aim to provide these data and insights to nurture future developments in this area. Accordingly, the risk assessments of our study were mainly focused on the lower technical level, i.e., implementing levels of redundancy in the vessel hardware, selecting industrially-robust components, having the ability to remotely control the vessel, and implementing emergency stops. In addition, the relatively small weight, and slow manoeuvring speeds add to a higher safety during the conducted experiments. Apart from these technical safety measures, the Flemish waterway administrator and by extent the Flemish government have taken an active role in the discussions regarding safety and regulations during the experiments conducted with our scale model vessel. They achieved this role by defining, monitoring, and continuously optimizing a legal framework for testing and demonstration purposes with autonomous inland vessels.

4.1. Navigational information

The navigational information such as position, orientation, velocity, etc., can be fetched by a standalone GNSS sensor, or a GNSS and an IMU separately, or an IMU with integrated GNSS corrections. Although the vessel desires a high accuracy from these sensors, the preciseness of their measurements can be influenced in practical applications due to environmental noise, sensor drift, and sensor faults (Liu et al., 2016). Moreover, the quality of GNSS signals will drop in the vicinity of tall buildings (Wang et al., 2012). Or, in the case of inland vessels, imperfect GNSS signals will occur in the neighbourhood of bridges, locks, quays, or other large vessels. Unfortunately, these are the situations where the highest accuracy would be desired. A first solution to diminish the effect of sensor faults and the impact of environmental noise, is to install state-of-the-art marine-grade sensors. Doing so, a GNSS and IMU, of which the specifications are discussed in sections 4.3.1 and 4.3.2, were selected and installed. The fusion of their data forms a second solution to increase their performance. Currently, an Extended Kalman Filter (EKF) based on the vessel kinematics improves the accuracy of the navigational data. Our future work aims at including the hydrodynamics of the vessel in a model based EKF, as for example in (Caccia et al., 2008; Tran et al., 2014).

4.2. Environment perception

Complementary to the necessity of accurate navigational information, an unmanned vessel needs to be aware of its surroundings which the authors divided into the aforementioned four separate cases, i.e. (I)-(IV). In the ideal environment of known, static obstacles and low or no environmental disturbances, an IMU and GNSS should suffice to autonomously navigate the vessel.

However, in order to perceive an unknown static object and its relative distance, a stereo camera, LIDAR, RADAR (RAdio Detection and Ranging), or a similar range measuring sensor has to be installed. LIDAR and, or, stereo camera based object detection has been a growing research field for indoor environments and the current research also expands towards, larger, outdoor environments, often forcing the sensor to collect data at a greater distance with a lower density (Grant et al., 2019). Although several successful studies have demonstrated the simultaneous localisation and mapping of an agent in a static environment, and some studies even implemented obstacle avoidance, e.g. (Hsu and Shiu, 2019; Zhang and Singh, 2017; Mousazadeh et al., 2018; Costa et al., 2016), it remains to be investigated which sensor set, and their minimum required specifications, is deemed necessary to achieve this goal on the inland waterways for cargo vessels.

Moreover, a supplementary challenge arises with the addition of dynamic objects as these also move or navigate in the ambient area and thus collision needs to be avoided.

An implementation of a COLREG compliant collision avoidance for dynamic objects can be found in Benjamin (2017), here the (autonomous) fleet can share navigational information with other (autonomous) vessels using the same nested MOOS-IvP software, hence making all the dynamic objects known. Given the fact that the Cogge uses the MOOS-IvP software, the usability of its obstacle avoidance implementation for inland waterways will be investigated via simulations in future work. Given the modularity of the software design, other collision avoidance strategies could also be implemented. Another example of an environment with known dynamic objects can be found in the Hull-to-Hull (H2H) navigation project (Kotzé et al., 2019; Berge et al., 2019) which also involves test cases with the Cogge. In this project, vessels share their navigational information and its uncertainty over a proprietary communication channel in order to perform close proximity encounters (see section 6.4). In addition, some navigational information of known dynamic obstacles can be fetched from the AIS data.

Nevertheless, in reality, not all vessels use their AIS, nor do all vessels have such a system, and different smaller waterway users can enter the operational environment of an unmanned vessel, unlocking the need of the detection and tracking of unknown dynamic objects. In comparison with their terrestrial and aerial robotic counterparts, there seem to be two main differences. On the one hand, most of the to-be-tracked objects tend to be larger in size exhibiting slower dynamics which could lower the complexity of tracking these objects. However, on the other hand, this also means that the objects have higher inertias and thus slower response times so the collision avoidance algorithms will need to operate and predict over a longer time horizon. This is a non-trivial task that needs to build its foundation on the results of (I)-(III), and consequently its complexity falls out of the scope of this study.

4.3. Selected sensors for the Cogge

During the first research stages, good weather conditions are presumed for the sensor selection. Later on, the additional complexity of bad weather conditions can be added. Keeping this assumption in mind, and based on the ongoing research mentioned above, the authors currently plan to investigate the usability of the sensor sets listed in Table 3 for the different environments. The following sections describe the selected onboard sensors (GNSS, IMU, LIDAR, and stereo cameras), and some intermediate results can be studied further down in section 6. The H2H proprietary communication protocols and media are not yet finalised, nor is an AIS currently installed, thus both systems will not be discussed in detail. Bear in mind that it is not unlikely that additional sensors will be added in the future, depending on the findings and possible limitations of the current sensor sets. On top of that, the achieved results in these environments can also help the development of more automated manned vessels. For example, these developments in the perception of the environment could guide, augment, or replace certain tasks currently performed by the onboard crew.

Table 3
Implemented and envisaged sensor settings on the Cogge.

Environment	Minimal sensor set	Status
Known, static obstacles (I)	GNSS, IMU	successful, see section 6.2
Unknown, static obstacles (II)	GNSS, IMU, LIDAR, stereo Camera	in progress, see section 6.3
Known, dynamic obstacles (III)	GNSS, IMU, AIS or proprietary communications	in progress, see section 6.4
Unknown, dynamic obstacles (IV)	GNSS, IMU, LIDAR, stereo Camera, AIS or proprietary communications	future work

4.3.1. GNSS

The installed AsteRx-U Marine GNSS sensor (Septentrio, 2017) can operate in temperatures ranging from −30 to 65 °C and has an IP67-rated housing, making it a robust sensor for inland vessels. On the Cogge, it uses two mushroom antennas (separated by a baseline of approximately 4.44 m) to receive multi-frequency and multi-constellation GNSS signals. This way, it can benefit from the more accurate European Galileo constellation while still being able to use additional constellations to boost its convergence time and accuracy (Li et al., 2015). Furthermore, it includes a ultra high frequency radio, Bluetooth, WiFi, and a cellular modem. This cellular connection allows for the reception of Real Time Kinematic (RTK) corrections (Langley, 1998) for the GNSS signals, drastically improving the accuracy of its navigational data. Table 4 summarises the impact of these RTK corrections on the performance of this sensor, together with other accuracies. As shown, the correction accuracy depends on the distance between the sensor and the nearest RTK base station. For example, for the horizontal position the absolute accuracy results in 0.6 cm + 0.05 cm per km of distance from the base station. Flanders currently has 45 base stations installed, ensuring a dense coverage, and freely provides these RTK corrections over mobile internet via the Flemish Positioning Service (Flepos, 2019).

4.3.2. IMU

The Ekinox-2-E IMU sensor can operate in the temperature range of −40 to 75 °C and has an IP68 rating (24 h submersible at 2 m) (SBG, 2018). This IMU uses three gyroscopes and three accelerometers to measure the angular velocities and linear accelerations of the vessel. Moreover, it can provide additional information regarding the position, orientation, and linear speeds of the vessel by means of single or double time integration. An internal kinematic EKF can be used to compensate for the IMU drift, shown by Fig. 12. The internal EKF predicts states at 200 Hz, based on the integration of its gyroscopes and accelerometers, and these states get a corrective step at 1 Hz provided by GNSS data from the AsteRx-U. An Ekinox-2-E software module first checks the integrity of this GNSS data and pulls it through its proprietary error model before sending it to the EKF.

Table 4
Absolute accuracies for the AsteRx-U Marine. Using the Twice the Distance Root Mean Square (2DRMS) accuracy: the distance between the true and computed parameter is lower than the stated accuracy with at least a 95% probability.

Parameter	Accuracy
Horizontal position, standalone	1.2 m
Vertical position, standalone	1. 9 m
Horizontal position, RTK	0.6 cm + 0.5 ppm
Vertical position, RTK	1.0 cm + 1 ppm
Velocity, standalone	0.03 m/s
Heading, 1 m baseline	0.15°
Heading, 10 m baseline	0.03°
Pitch, 1 m baseline	0.25°
Pitch, 10 m baseline	0.05°

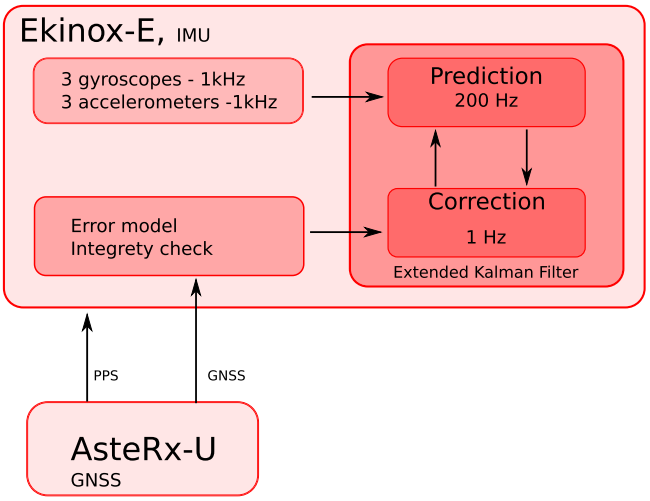

Fig. 12. Working principle of the EKF nested inside the IMU, based on (SBG, 2018).

The line of sight between the tracked satellites and the GNSS mushrooms will be disturbed and potentially blocked when, for example, passing a bridge. Consequently, it is of paramount importance for an unmanned vessel to still receive reliable navigational information during this time span. Table 5 demonstrates two examples of the importance of the EKF by listing its accuracy in function of the elapsed time since a corrective GNSS signal was received (0s, 10s, and 30s). Logically, the accuracy diminishes the longer a GNSS outage lasts. Nevertheless the Ekinox-2-E is still capable to produce useful data during these shorter outages which align with the typical time of passing under a bridge. Furthermore, the IMU computes and publishes the accuracies of its predicted states so that an autonomy system could take this into account.

4.3.3. LIDAR

The OPAL 1000 LIDAR has no external moving parts, sits in an IP67 housing, and can operate in −40 to 40 °C (Neptec, 2019). The laser scanner measures a panoramic field of view of 360° in the horizontal plane, and 45° in the vertical plane, at a maximum rate of 300 000 pulses per second, with a maximum range of 1000 m. It can penetrate obscurants such as dust, snow, rain, fog, and smoke by using its patented algorithm which uses 7 pulses to measure one point. Moreover, it can also be connected to, and synced with, the IMU and GNSS in order to perform scans while the vessel is moving.

4.3.4. Cameras

A computer vision technology company named Vision++ provided the tailored stereo camera system (Vision++, 2019). This system consists of two industrial cameras positioned on the port and starboard side of the bow sensor rail. Most conventional, commercially available, systems have a maximum distance of 40 cm between both cameras, whereas on the Cogge, they have a baseline of 60 cm which provides an optimal depth sight at a distance of approximately 15–20 m, i.e. 3-4 times the length of our scale model. These cameras have a frame rate of 22 frames per second, a pixel class of 5 megapixel, and a Power-Over-Ethernet connection which simplifies the power and communication requirements. When creating stereoscopic images, it is crucial that the images provided by both cameras are taken simultaneously. Hence, in the current set-up, the cameras are connected to each other via a proprietary wire allowing one camera to trigger the other camera on receipt of the command to record an image. The camera software suite controls the cameras and allows the user to fine tune the settings of the cameras to optimize their exposure. In addition, the software supplied by Vision++ enables the extraction of 3-dimensional-point cloud data from a stereo camera image, specifically configured for an inland waterway environment. This is to be used in conjunction with the point cloud data produced by the LIDAR, but raw camera images will also be used to aid environment perception and obstacle detection.

Table 5
Accuracy of the IMU dependent on GNSS outages, one standard deviation.

Parameter	Accuracy
Horizontal velocity, 0s	0.02 m/s
Horizontal velocity, 10s	0.05 m/s
Horizontal velocity, 30s	0.25 m/s
Heading (baseline > 4 m) 0s	0.05°
Heading (baseline > 4 m) 10s	0.08°
Heading (baseline > 4 m) 30s	0.13°

5. Motion control

As explained in section 3.4.2, three levels of control make up the total software design for the motion control of the vessel. Fig. 13 summarises the main interactions between these three (low, middle, and high) control levels for an example configuration when the Cogge follows a list of waypoints. These three control levels are further clarified by sections 5.1, 5.2, and 5.3 with reference to Fig. 13.

5.1. High level control

The high level control covers the top-level route planning, for example the determination of the route to be taken between two cities. Currently, an in-house developed waypoint generator forms a static list of waypoints between a configured start and endpoint on a river or canal. This developed generator uses the OpenStreetMaps (OpenStreetMap Contributors, 2019) database in order to fetch the global coordinates from the chosen waterway. The generator places waypoints in the middle of the waterway, and the maximum distance between two consecutive waypoints can be specified by the user. Finally, the result can be downloaded as a plain text file and be used as to-be-tracked waypoints by the middle level control.

5.2. Middle level control

The MOOS-IvP autonomy system provides the foundation for the middle level control for the Cogge. Three main components form the core of this autonomy system: a collection of MOOSApps, the autonomy decision making IvP-helm (which is a MOOSApp on its own), and the MOOSDB for their communication. To configure the IvP-helm, the user can write or use a set of behaviors that the vessel should follow, for example: follow waypoints and maintain a certain speed. These behaviors have IvP-functions, defined by the user, which span over their decision space (e.g. heading, speed, …). Moreover, the user can also decide when a particular behavior should occur by configuring the mission modes. The IvP helm will calculate the optimal system states depending on the different behaviors, and their weighted IvP-functions. More in-depth information can be found in Benjamin et al. (2010).

Continuing with the illustrative configuration of Fig. 13, the IvP-helm could be configured to, for example, solely follow waypoints by using the MOOS-IvP waypoint-following behavior. This behavior needs a list of waypoints to follow, which in this case will be provided by the aforementioned high level control. Next, the IvP-helm needs navigational information, e.g. the current heading and speed, to calculate the desired heading and speed for the Cogge to reach the following waypoint. This information flow illustrates the backseat control paradigm: the autonomy decision making IvP Helm only needs navigational information form the vessel at hand, which he can treat as a black box, and will then, based on its internal behavior configuration, provide the

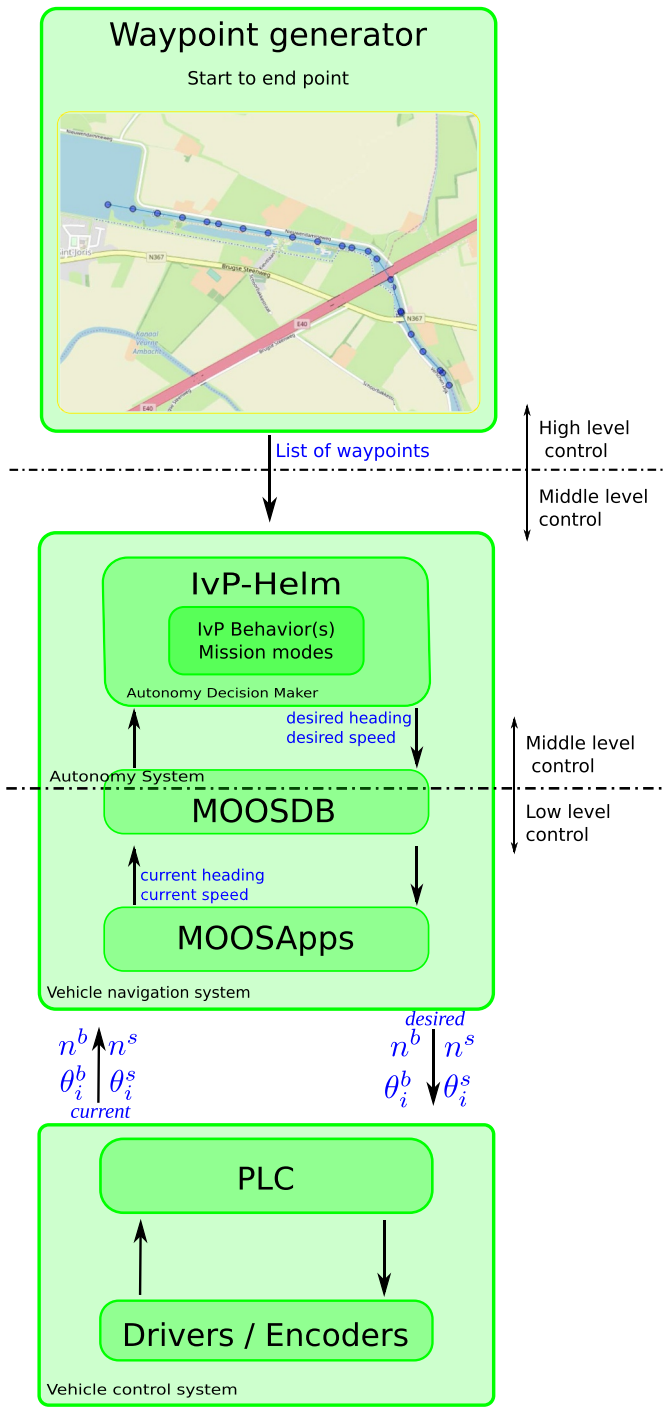

Fig. 13. Implemented control hierarchy.

desired systems states for this vessel. Nevertheless, in the control architecture of the Cogge, the navigation and control modules are no black boxes but also consist of several MOOSApps, such as drivers for the sensors and the low level motion controller. Therefore, the virtual hierarchical separation line between middle and low level control has been drawn at the level of the MOOSDB as some part of the autonomy system (the IvP-Helm and its surroundings) form the middle level control and other parts (low level motion controller and sensor drivers) form the low level control and vehicle navigation system.

5.3. Low level control

The low level control diminishes the error between the desired and current system states, e.g. the heading and speed. The former states are produced by the middle level control and the latter are provided by the GNSS and IMU sensors. Currently, a conventional Proportional Integral Derivative (PID) controller is implemented as a MOOSApp to control the heading and total speed of the vessel, hence to control the Cogge in two degrees of freedom on the water plane. The PID controller is a well-known, simple, and robust controller often used in maritime applications, although more advanced controllers exist which take the kinematics into account as discussed in, for example (Do and Pan, 2009), and (Fossen, 2011). Nevertheless, the performance of this PID controller can be used as a benchmark for the future implementation of more sophisticated control philosophies. Finally, the PLC receives the output of the PID controller, i.e. the desired control system states, $n^b, n^s, \theta_i^b, \theta_i^s$, communicates with their respective drivers, and sends back their current values (see section 3.4.1).

6. Results and discussion

This section analyses some of the first experiments conducted with the Cogge. First, section 6.1 demonstrates a few open-loop experiments to uncover some of the basic hydrodynamic capabilities of the vessel. These trials were performed on the small lake of Rotselaar, Belgium. Afterwards, the subsequent sections discuss a few different environment interactions in the aforementioned differentiated cases (I), (II), and (III).

6.1. Open-loop, Rotselaar lake

6.1.1. Straight sailing

During the first open-loop tests the Cogge showed an asymmetric course behaviour. When the vessel was commanded to sail straight (e.g. giving solely the stern an rpm, i.e. $n^s \neq 0$ and $n^b = \theta_i^b = \theta_i^s = 0$) it seemed to show a repetitive asymmetric behaviour which turned the vessel to starboard. Presently, it is hard to discover the exact cause of this behaviour. A first empirical solution was to place a honeycomb-like flow-straightener in the longitudinal direction of the stern-side outlet of the stern thruster to straighten its exiting water flow when sailing straight ahead. Fig. 14 displays the effect of this flow-straightener on the straight line sailing capacity of the vessel. The black lines show the first experiments without flow-straightener, whereas the red lines show similar experiments but with the flow-straightener inserted in the stern

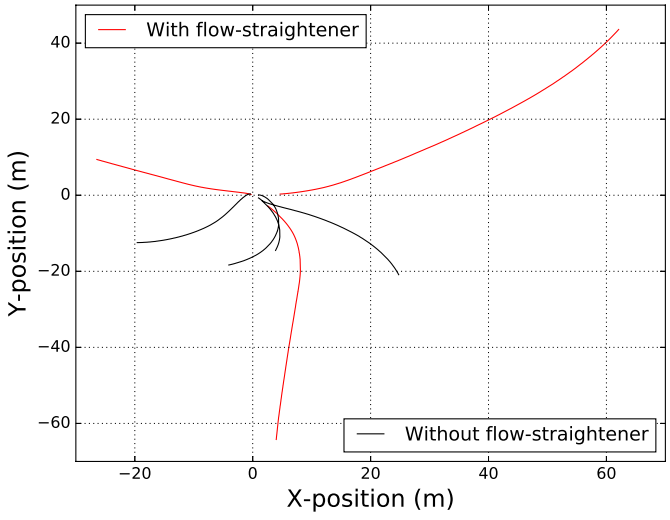

Fig. 14. Sailed trajectories for open-loop straight sailing with and without flow-straightener, the positions were measured by the GNSS placed at the stern.

outlet. Note how the black lines show a high curvature due to the asymmetric behaviour, whereas the red lines show a more linear sailing behaviour over longer spatial slots. The differences in length between all curves are due to different requested propeller speeds and time spans of the missions. The installation of this flow straightener significantly improved the straight line stability of the vessel, which can also be felt when the remote control is used to steer the vessel.

6.1.2. Pseudo spiral manoeuvre

To investigate the possible turning rates of the Cogge, a pseudo spiral manoeuvre was performed. This manoeuvre slightly differs form the Dieudonné spiral manoeuvre (Dieudonné, 1953) as the vessel only turned into one direction and there was a constant settling time between the rudder impulses. The uncertainty of the spatial necessities for a full spiral manoeuvre pushed the decision to, initially, only perform such a pseudo spiral manoeuvre. The manoeuvre was performed fully autonomous with the following desired settings: $n^s = 1000\ rpm$, $\theta_i^s = 0°$, $n^b = 2500\ rpm$, and θ_i^b varying between $[4, 8, 20, 40, 60, 80]°$. Hence the stern thruster was oriented to propel the vessel forward (with the flow-straightener installed) and the bow thruster was used to steer by using a constant propeller speed but changing its outlet angle. Fig. 15(a) lists these desired system states during the whole mission. As visible, an arbitrarily settling time of 10 s was used, this time span was chosen to be rather short in order to have the space to perform the mission, but it can be increased in future tests. For the same reason, the first angle change occurred right from the start, introducing some start-up effects in the data as the vessel itself also needed to accelerate. In the future a longer start-up time could be introduced. Fig. 15(b) plots the measured course from the GNSS and the recorded yaw-rates from the IMU. The latter were filtered with a centered moving average filter of window size 50. Finally, Fig. 15(c) plots the sailed trajectory.

6.2. Environment I: known, static obstacles

6.2.1. Autonomous sailing on the Yzer river

The first autonomous, unmanned, closed-loop tests were performed on the Yser in Nieuwpoort, Belgium, in the context of the EFRO (European Fund for Regional Development) project "Autonoom Varen in de Westhoek". This EFRO project investigated the legal and technical necessities to perform a pilot demonstration of autonomous sailing with a scale model of an inland vessel in a confined demonstration area. Afterwards the project conducted such tests of which the described tests in this section were the first ones. These preliminary tests used the control hierarchy described in section 5. Moreover, the map shown in the waypoint generator of Fig. 13 actually shows some of the generated waypoints for these experiments. After the generation of the waypoints list, and the implementation of the IvP-Helm to follow these consecutive waypoints, the low level controller needs to be configured. The angle of the bow thruster provided the steering mechanism for the vessel, whereas the stern thruster was kept a static neutral angle. This set-up aligns with the configuration of section 6.1.2 and had the following settings: $n^s = 1250\ rpm$, $\theta_i^s = 0$, $n^b = 2400\ rpm$, and $\theta_i^b \in [-90, 90]°$ as control variable. The IvP-helm provided the desired heading to follow the waypoints and the IMU gave the current heading. The error between both headings was controlled with a manually tuned PI-control on θ_i^b, with a proportional gain factor $K_P = 2$ and an integral gain factor $K_I = 0.2s^{-1}$ with an integral limit of 0.7 in order to avoid integral wind-up.

Fig. 16 summarises two parts of autonomous sailing on the Yser: (a), (b), and (c) show a fragment of a straight part on the Yser, whereas (d), (e), and (f) show a sample of a bend of the Yser whilst passing under a bridge. These two samples are also visible on the map of Fig. 13 where the red line is the highway bridge under which the vessel sailed in (d). The plotted waypoints of (a) and (d) have a higher density than the waypoints of Fig. 13, as for the latter the amount of visible waypoints was decreased to increase the readability of the figure. Next, plots (b)

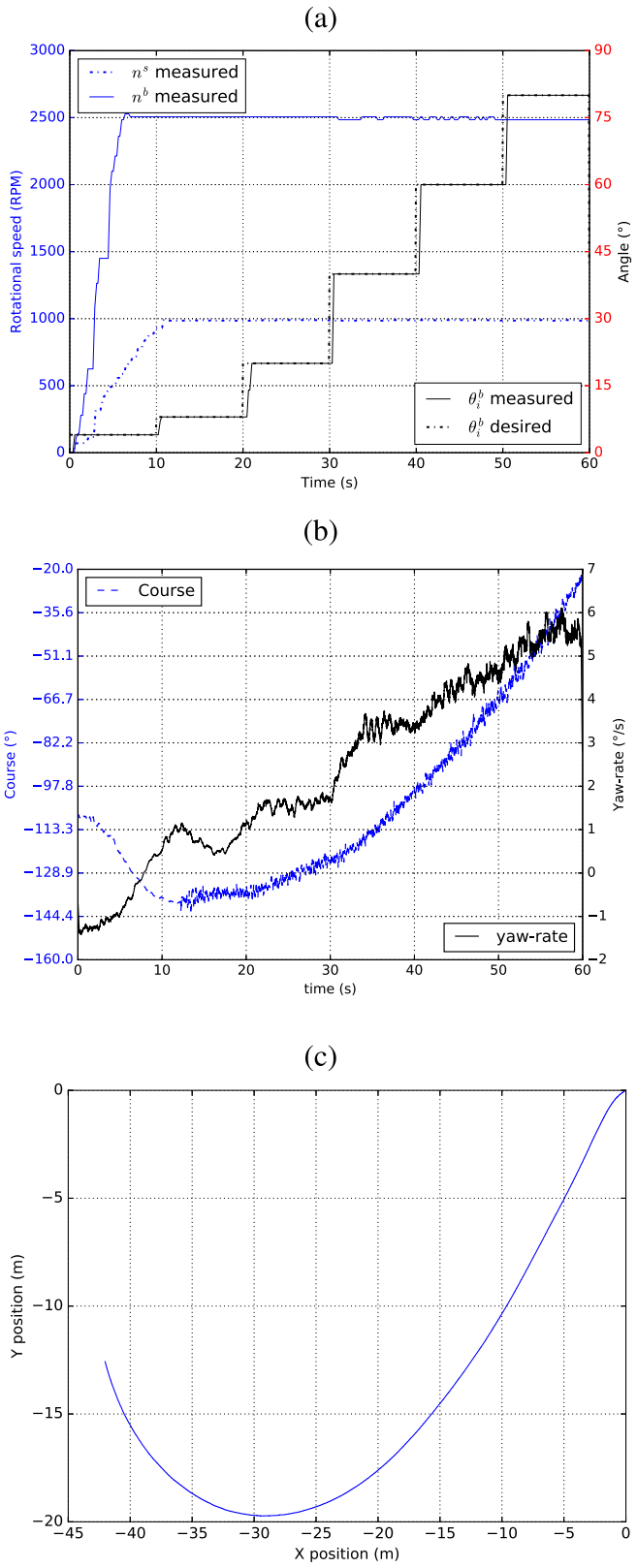

Fig. 15. Open-loop pseudo spiral manouevre: (a) manoeuvre inputs, (b) relevant system outputs, and (c) elapsed trajectory, the positions were measured by the GNSS placed at the stern.

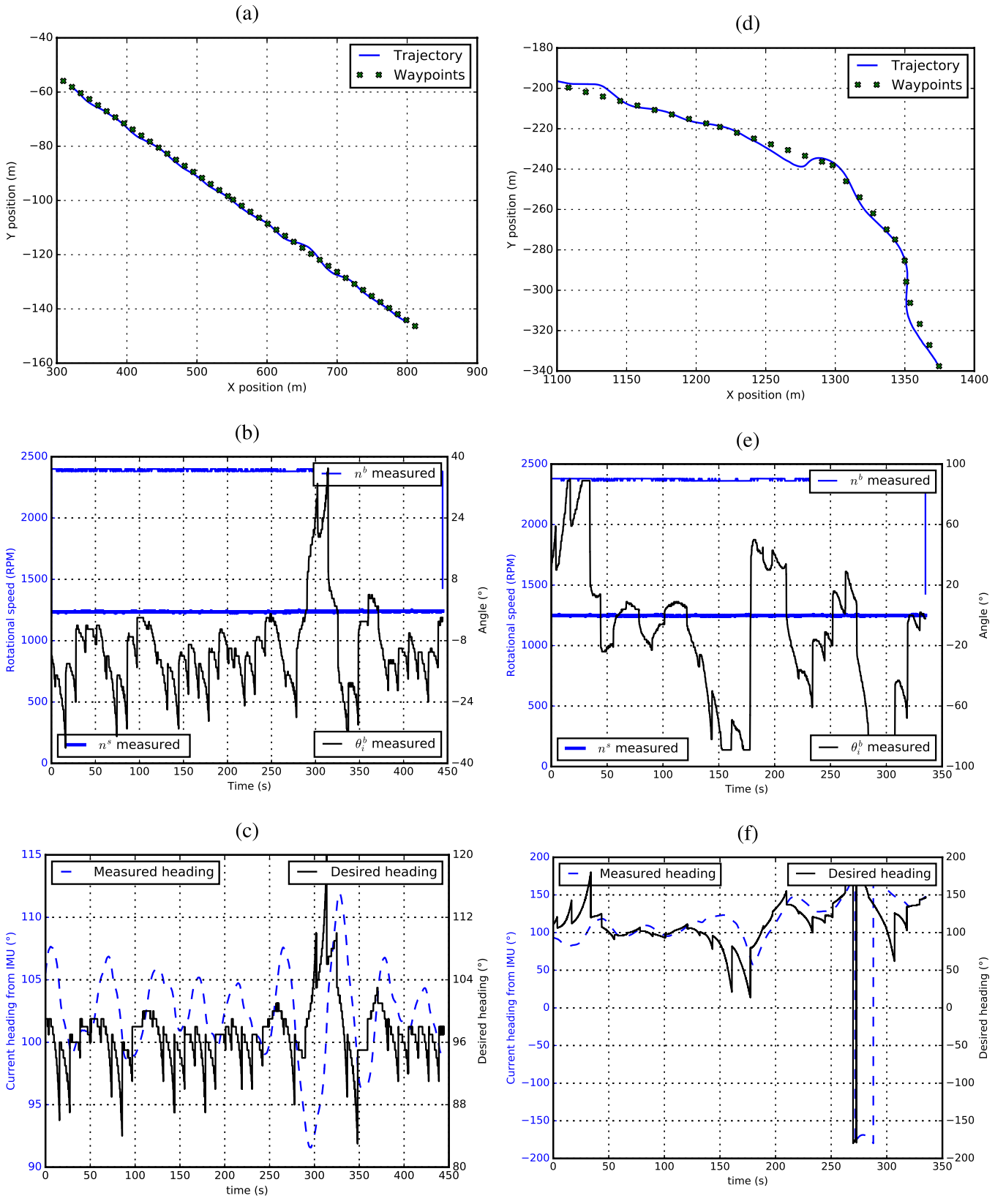

Fig. 16. Closed loop waypoint following on the Yser. Straight trajectory on the left (a-b-c) and curved trajectory on the right (d-e-f), the positions were measured by the GNSS placed at the stern.

and (e) show the measured propeller speeds on the one hand, and the measured control angle, θ_i^b, on the other hand. Finally, (c) and (f) show the desired heading, published by the IvP-Helm, and the current heading, fetched from the IMU. Note that these headings are shown within the boundaries of [-180, 180]°, which causes the sudden change from 180° to −180° in (f). As demonstrated by these six subplots, the vessel was able to follow the waypoints on both a straight and curved trajectory.

6.3. Environment II: unknown, static obstacles

6.3.1. LIDAR scans

Fig. 17 illustrates a static scan with an exposure of 5 min at the small inland leisure harbour of Leuven, Belgium, where the LIDAR was placed on the shoreside. On the left side of this image, a few moored leisure craft can be seen. Fig. 18 shows the accumulated data of an approximately 1 min scan while the vessel was slowly sailing. The left hand side plots the raw LIDAR data using a color code from red to blue to denote the decreasing intensity of the measured points, and thus increasing distance relative to the LIDAR. The right hand side of the figure plots the manual overlay of the LIDAR data (now in black) on the local geographical map of the lake of Rotselaar where these data were fetched. Hence for this configuration the LIDAR was mounted on the vessel and had access to the IMU data. During the exposure time, a windsurfing class was also present on the water which resulted in the ghost points on the water close to the top of the image.

6.3.2. Stereo camera images

Fig. 19 depicts two, simultaneously-taken, images of the stereo camera system. The visible railway bridge lies at the coordinates (50°54′01.5″N, 4°42′23.9″E). As mentioned in section 4.3.4, these images can be used to extract depth data of the surrounding environment. The images were taken on a rainy day where water droplets eventually made it onto the lenses, resulting in the blurred result. This effect of the weather shows the importance of using more than one perception system and hints at the future research challenges when the effects of bad weather conditions are added.

6.3.3. In-operation communication data rates

The following data rates indicate the measured data consumptions during the experiments discussed in section 6. Evidently, they depend on the configuration of certain sensor parameters. In order to avoid confusion, two separate network loops can be detailed: (i) the local network, i.e. communication between the sensors and the onboard I-PC, and (ii) wireless vessel-to-shore communication, i.e. where certain data could be transmitted between the onboard I-PC and the shoreside R–PC.

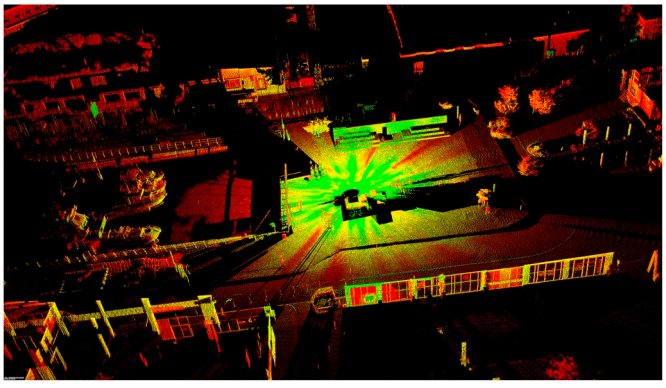

Fig. 17. LIDAR cloud after 5 min of exposure time with the OPAL 1000. The shown area is approximately 50 m by 100 m, on the left the bow of a few leisure vessels can be seen and on the right some trees. The top and bottom show the contours of the neighbouring buildings.

In the first case, both the GNSS and IMU consume less than 1 Mbps (Megabit per second). The LIDAR uses approximately 5 Mbps when it spins on one-sixth of its maximum frequency. And, given that each camera can produce 5 megapixel images at 22 frames per second, they could theoretically each approximately produce a maximum data rate of 330 Mbps which they can each transmit over a category seven Ethernet cable.

In the second case, when one wants to stream some of these data wirelessly to another device, there are currently two options available via the onboard router: using the cellular network or using a Wireless Local Area Network (WLAN). Note that this router has a theoretical maximum bandwidth of 150 Mbps. On top of that, the current cellular 4G network has a claimed maximum bandwidth of 100 Mbps. However, this number is highly environment dependent and a conservative bandwidth of 5-15 Mbps was noticed to be more representative for the possible regime data rates at our testing locations. During the experiments, there was always a wireless communication between the onboard MOOS processes and the MOOS processes on a remote laptop which triggered and monitored their onboard counterparts. The frequency and the content of these vessel-to-shore communications can be chosen and was never larger than 1 Mbps, hence it was always possible to transmit these data over the cellular network. The authors plan to add a second, separated local network to route all the data coming from the perception sensors, together with a second I-PC to process all these data and a second router to transmit this data if desired.

6.4. Environment III: known, dynamic obstacles

In the European Horizon 2020 project “Hull-to-Hull (H2H)”, the Cogge will be deployed in an environment with known dynamic objects (Kotzé et al., 2019). This H2H concept uses uncertainty zones to visualise the relative positioning between H2H-compliant vessels (Berge et al., 2019). This project is a cooperation between Kongsberg Seatex AS (NO), SINTEF Ocean AS (NO), SINTEF Digital (NO), Mampaey Offshore Industries (NL) and KU Leuven (BE). The H2H project has received funding from the European GNSS Agency under the European Union’s Horizon 2020 research and innovation programme grant agreement No 775998.

7. Conclusions and future work

This paper discussed the design of an experimental platform which aims to help study the feasibility and current or future limitations of unmanned inland cargo vessels. The authors believe that the developed platform can provide indispensable technological information which can steer the investigation of possible business cases for more automated or unmanned inland cargo vessels. To achieve this goal, the focus was put on the three following design aspects:

(i) *Industrial relevance.* The newly introduced fleet of self-propelled Watertruck$^+$ barges inspired the design of the scale model, and its size fits the research potential for urban water freight transport. Furthermore, the over-actuated propulsion system which has two 360-degrees-steerable thrusters offers the possibility of advanced motion control philosophies, while it can also serve to mimic under-actuated propulsion systems. In addition, the selection of marine-grade, industrially-robust, state-of-the-art sensors offer insights for vessels in real-operation and could even be transferred to a real-size vessel with minimal necessary changes. Finally, the focus on modularity in both the hardware and software design offers redundancy, genericness, and facilitates further research.

(ii) *Interactions with the environment.* The perception of, and the interaction with, different environments were split into four cases handling known or unknown, static or dynamic obstacles. Afterwards, the technological challenges for these environments

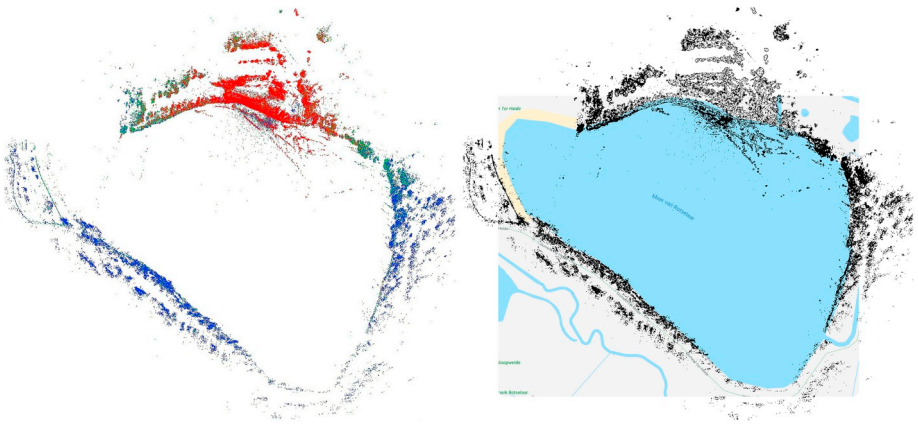

Fig. 18. LIDAR data from an approximately 1 min scan while the vessel was moving: (left) intensity data points, (right) manual overlay of data on geographical map.

(a) (b)

Fig. 19. (a) image of the left camera, (b) image of the right camera, taken at the same time stamp.

were examined which resulted in the selected sensor sets and their specifications. Complementary, preliminary results for environments (I), (II), and (III) were presented.

(iii) *Motion Control.* The cascaded motion control philosophy, consisting of three levels, provides the flexibility to study different implementations of these distinct levels. Moreover, the instrumented backseat driver paradigm makes the decision making part of the motion control vessel independent. An experiment conducted on the Yzer river, illustrated the successful implementation of the cascaded motion control design, ranging from the human scheduling input to the lowest actuation control signals controlled by the PLC.

In conclusion, the integration of these design aspects resulted in the blueprint for an unmanned inland cargo vessel which successfully performed preliminary unmanned and autonomous experiments. Although these experiments were fruitful, further improvements will be key to study the potential of operating unmanned inland cargo vessels. Therefore some of the on-going research of the authors is currently oriented towards:

(i) The modelling and identification of both propulsion systems, with a special focus on the thrust deduction losses due to the fact that both propellers are completely nested inside the hull and rotate in a plane parallel with the calm water plane.

(ii) The identification of hydrodynamic motion models which could serve as plant or control models depending on their complexity.

(iii) The development of advanced low, middle, and high level motion controllers, where the full flexibility and, or, identification of the actuation system at hand can be used.

(iv) The further development of the perception of the environment on the basis of the selected sensor sets. Moreover, additional sensors can be added in the future such as a weather station, speed over water sensor, or RADAR.

(v) The alignment and integration of the developed solutions with the existing AIS and RIS.

This future work list does not exhaust all the technological challenges that lie ahead, but demonstrates their vast amount in order to achieve increasingly automated or even unmanned inland cargo vessels. Nevertheless, this study validated a first working example of an unmanned inland cargo vessel operating in a-priori known environment with static obstacles, and provided preliminary results and insights for the dynamic and unknown environments.

Author contributions

Gerben Peeters: Conceptualization, Methodology, Software, Validation, Investigation, Writing – Original Draft.

Marcus Kotze: Conceptualization, Validation, Investigation.

Muhammad Raheel Afzal: Validation, Investigation, Writing – Review & Editing.

Tim Catoor: Conceptualization, Software, Validation, Investigation.

Senne Van Baelen: Conceptualization, Software, Validation, Investigation.

Patrick Geenen: Conceptualization, Validation, Investigation.
Maarten Vanierschot: Writing – Review & Editing, Supervision.
Rene Boonen: Supervision.
Peter Slaets: Conceptualization, Supervision, Project Administration, Funding acquisition.

Declaration of competing interest

The authors declare that they have no known competing financial interests or personal relationships that could have appeared to influence the work reported in this paper.

Acknowledgments

The Flanders Research Foundation (FWO) funds the doctoral scholarship of Gerben Peeters [1S12517N]. The scale model was funded by the EFRO-Flanders project “Autonoom Varen in de Westhoek”.

Appendix

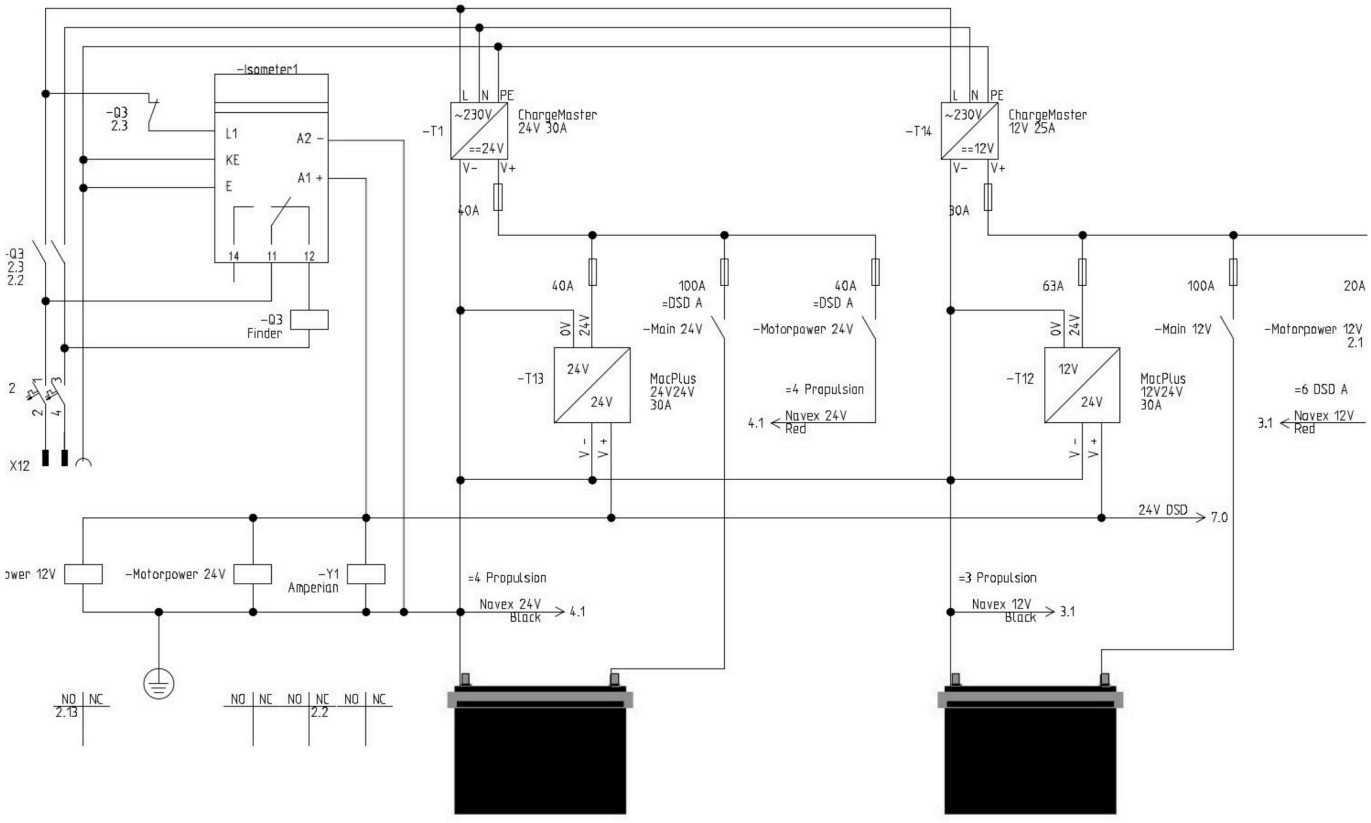

Power supply and charging system

Power supply and charging system.

References

Abilio Ramos, M., Utne, I.B., Mosleh, A., 2019. Collision avoidance on maritime autonomous surface ships: operators’ tasks and human failure events. Saf. Sci. 116 (March), 33–44. https://doi.org/10.1016/j.ssci.2019.02.038. URL.

Al Enezy, O., van Hassel, E., Sys, C., Vanelslander, T., 2017. Developing a cost calculation model for inland navigation. Res. Transp. Bus. Manag. 23, 64–74. https://doi.org/10.1016/j.rtbm.2017.02.006. URL.

Benjamin, M.R., 2016. Trends in marine vehicles technologies affecting autonomy. URL. https://oceanai.mit.edu/ivpman/pmwiki/pmwiki.php?n=Helm.MarineTechnologiesname.

Benjamin, M.R., 2017. Autonomous COLREGS Modes and Velocity Functions Autonomous COLREGS Modes and Velocity Functions. Tech. rep.. MIT-CSAIL.

Benjamin, M.R., Schmidt, H., Newman, P.M., Leonard, J.J., nov, 2010. Nested autonomy for unmanned marine vehicles with MOOS-IvP. J. Field Robot. 27 (6), 834–875. https://doi.org/10.1002/rob.20370. URL.

Berge, S.P., Hagaseth, M., Kvam, P.E., 2019. Hull-to-Hull positioning for maritime autonomous ships (MASS). In: 18th Conf. Comput. Appl. Inf. Technol. Marit. Ind., pp. 314–323.

Bertram, V., 2008. Unmanned surface vehicles – a survey. In: Ski. Selsk, pp. 1–14. URL. http://www.skibsteknisk selskab.dk/public/dokumenter/Skibsteknisk/Downloadmateriale/2008/10marts08/USVsurvey_DTU.pdf.

Caccia, M., Bibuli, M., Bono, R., Bruzzone, G., 2008. Basic navigation, guidance and control of an unmanned surface vehicle. Aut. Robots 25 (4), 349–365.

Campbell, S., Naeem, W., Irwin, G.W., 2012. A review on improving the autonomy of unmanned surface vehicles through intelligent collision avoidance manoeuvres. Annu. Rev. Contr. 36 (2), 267–283. https://doi.org/10.1016/j.arcontrol.2012.09.008. URL.

Caris, A., Limbourg, S., Macharis, C., van Lier, T., Cools, M., 2014. Integration of inland waterway transport in the intermodal supply chain: a taxonomy of research challenges. J. Transport Geogr. 41, 126–136.

CEMT, 1992. Resolution No.92/2: on New Classification of Inland Waterways. Tech. Rep. 92. European Conference of Ministers of Transport.

Costa, C.M., Sobreira, H.M., Sousa, A.J., Veiga, G.M., 2016. Robust 3/6 DoF self-localization system with selective map update for mobile robot platforms. Robot. Autonom. Syst. 76, 113–140. https://doi.org/10.1016/j.robot.2015.09.030. URL.
Dieudonné, J., 1953. Collected French Papers on the Stability of Route of Ships at Sea, 1949-1950, (Translated by H. E. Saunders and E. N. Labouvie). Technical Report DTMB-246.Naval Ship Research and Development Center. Washington D.C. Tech. rep. Naval Ship Research and Development Center.
Do, K.D., Pan, J., 2009. Control of Ships and Underwater Vehicles. Springer.
European Commission, 2018a. TEN - T. Tech. Rep. European Commission. URL. https://ec.europa.eu/transport/about-us_en.
European Commission, 2018b. Watertruck+ project. URL. www.watertruckplus.eu.
European Commission, 2019. Eurostat. Tech. Rep. European Commission. URL. https://ec.europa.eu/eurostat/data/database.
Flepos, 2019. Flepos. URL. https://overheid.vlaanderen.be/flepos-algemeen.
Fossen, T.I., 1994. Guidance and Control of Ocean Vehicles. Wiley, New York.
Fossen, T.I., 2002. Marine Control Systems Guidance, Navigation, and Control of Ships, Rigs and Underwater Vehicles. Marine Cybernetics, Trondheim, Norway.
Fossen, T.I., 2011. Handbook of Marine Craft Hydrodynamics and Motion Control. John Wiley & Sons.
Grant, W.S., Voorhies, R.C., Itti, L., 2019. Efficient Velodyne SLAM with point and plane features. Aut. Robots 43 (5), 1207–1224. https://doi.org/10.1007/s10514-018-9794-6. URL.
Hsu, C.M., Shiu, C.W., 2019. 3D LiDAR-based precision vehicle localization with movable region constraints. Sensors 19 (4).
Janjevic, M., Ndiaye, A.B., 2014. Inland waterways transport for city logistics: a review of experiences and the role of local public authorities. WIT Trans. Built Environ. 138, 279–292.
Kalikatzarakis, M., Geertsma, R.D., Boonen, E.J., Visser, K., Negenborn, R.R., 2018. Ship energy management for hybrid propulsion and power supply with shore charging. Contr. Eng. Pract. 76 (November 2017), 133–154. https://doi.org/10.1016/j.conengprac.2018.04.009. URL.
Kallas, S., 2011. Transport 2050: Commission Outlines Ambitious Plan to Increase Mobility and Reduce Emmisions. Tech. Rep. March. European Commission. URL. http://europa.eu/rapid/press-release_IP-11-372_en.htm.
Kotzé, M., Junaid, A.B., Afzal, M.R., Peeters, G., Slaets, P., 2019. Use of uncertainty zones for vessel operation in inland waterways. J. Phys. Conf. Ser.
Laine, B., Hoornaert, B., Coraline, D., 2019. Transportvraag in België. Tech. Rep. December. Federaal Planbureau, Brussel.
Langley, R.B., 1998. Rtk Gps, vol. 104. Gps World, pp. 70–76. URL. http://yokoya.aist-nara.ac.jp/paper/datas/835/miru2005_2.pdf.
Lataire, E., Vantorre, M., Delefortrie, G., 2018. The influence of the ship's speed and distance to an arbitrarily shaped bank on bank effects. J. Offshore Mech. Arctic Eng. 140 (2), 021304.
Li, X., Ge, M., Dai, X., Ren, X., Fritsche, M., Wickert, J., Schuh, H., 2015. Accuracy and reliability of multi-GNSS real-time precise positioning: GPS, GLONASS, BeiDou, and Galileo. J. Geodyn. 89 (6), 607–635. https://doi.org/10.1007/s00190-015-0802-8. URL.
Liu, J., Hekkenberg, R., Quadvlieg, F., Hopman, H., Zhao, B., 2017. An integrated empirical manoeuvring model for inland vessels. Ocean. Eng. 137 (September 2016), 287–308. https://doi.org/10.1016/j.oceaneng.2017.04.008. URL.
Liu, J., Hekkenberg, R., Rotteveel, E., Hopman, H., 2015. Literature review on evaluation and prediction methods of inland vessel manoeuvrability. Ocean. Eng. 106, 458–471. https://doi.org/10.1016/j.oceaneng.2015.07.021. URL.
Liu, Z., Zhang, Y., Yu, X., Yuan, C., 2016. Unmanned surface vehicles: an overview of developments and challenges. Annu. Rev. Contr. 41 (May), 71–93.
Maes, J., Sys, C., Vanelslander, T., 2012. Vervoer te water: linken met stedelijke distributie? Tech. Rep., Steunpunt Goederen-en personenvervoer.
Manley, J., 2008. Unmanned surface vehicles, 15 Years of development. In: MTS/IEEE Ocean, pp. 1–4, 2008.
Megumi, S., Susumu, O., 2019. Considerations on the regulatory issues for realization of maritime autonomous surface ships considerations on the regulatory issues for realization of maritime autonomous surface ships. In: J. Phys. Conf. Ser. IOP Publishing.
Midjas, T., 2018. Collision Avoidance for the ReVolt Model-Scale Ship. Masther thesis. NTNU.
Moreira, L., Guedes Soares, C., 2011. Autonomous ship model to perform manoeuvring tests. J. Marit. Res. 8 (2), 29–46.
Mousazadeh, H., Jafarbiglu, H., Abdolmaleki, H., Omrani, E., Monhaseri, F., reza Abdollahzadeh, M., Mohammadi-Aghdam, A., Kiapei, A., Salmani-Zakaria, Y., Makhsoos, A., 2018. Developing a navigation, guidance and obstacle avoidance algorithm for an Unmanned Surface Vehicle (USV) by algorithms fusion. Ocean. Eng. 159 (January 2017), 56–65. https://doi.org/10.1016/j.oceaneng.2018.04.018. URL.
MUNIN, 2016. Maritime unmanned navigation through intelligence in networks (MUNIN). URL. http://www.unmanned-ship.org/munin.
Neptec, 2019. User Manual and Guide OPAL Perfomande Series 3D LiDAR Scanner. Tech. Rep. May. Neptex Technologies Corp.
Newman, P.M., 2005. {MOOS} - Mission Orientated Operating Suite. Tech. Rep. March. MIT.
OpenStreetMap Contributors, 2019. OpenStreetMap. URL. https://www.openstreetmap.org.
Peeters, G., Catoor, T., Afzal, M.R., Kotze, M., Geenen, P., Van Baelen, S., Vanierschot, M., Boonen, R., Slaets, P., 2019. Design and build of a scale model unmanned inland cargo vessel : actuation and control architecture. J. Phys. Conf. Ser.
Pompée, P.-J., 2015. About modelling inland vessels resistance and propulsion and interaction vessel - waterway. PIANC Smart Rivers 2015 (September), 7–11.
Rødseth, Ø.J., 2015. D10 . 1 : Impact on Short Sea Shipping. Tech. rep.. MRTK.
Rødseth, Ø.J., Nordahl, H., 2018. Norwegian Forum for. Tech. Rep. August. SINTEF Ocean AS.
Savitz, S., Blickstein, I., Buryk, P., Button, R.W., DeLuca, P., Dryden, J., Mastbaum, J., Osburg, J., Padilla, P., Potter, A., Price, C.C., Thrall, L., Woodward, S.K., Yardley, R. J., Yurchak, J.M., 2013. U.S Navy Employment Options for Unmanned Surface Vehicles. Tech. rep.. National Defense Research Institute. URL. https://www.rand.org/content/dam/rand/pubs/research_reports/RR300/RR384/RAND_RR384.pdf.
SBG, 2018. Ekinox Surface Series Tactical Grade MEMS Inertial Sensors Hardware Manual. Tech. rep.. SBG Systems.
Septentrio, 2017. AsteRx-U User Manual. Tech. rep.. Septenrio, Leuven.
Vanelslander, T., Sys, C., 2011. Future Challenges for Inland Navigation. Vub University Press.
Thieme, C.A., Utne, I.B., Haugen, S., 2018. Assessing ship risk model applicability to marine autonomous surface ships. Ocean. Eng. 165 (July), 140–154. https://doi.org/10.1016/j.oceaneng.2018.07.040. URL.
Tran, N.-h., Choi, H.-s., Baek, S.-h., Shin, H.-y., 2014. AETA 2013: recent advances in electrical engineering and related sciences. Rec. Adv. Electr. Eng. Relat. Sci. 282, 575–584. URL. http://link.springer.com/10.1007/978-3-642-41968-3.
Valdez Banda, O.A., Kannos, S., Goerlandt, F., van Gelder, P.H., Bergström, M., Kujala, P., 2019. A systemic hazard analysis and management process for the concept design phase of an autonomous vessel. Reliab. Eng. Syst. Saf. 191.
Vallant, J., Hofmann-Wellenhof, B., 2008. River information services. Elektrotechnik und Informationstechnik 125 (6), 238–243.
van Essen, H., 2018. Sustainable Transport Infrastructure Charging and Internalisation of Transport Externalities. Tech. Rep. December. CE Delft. URL. https://ec.europa.eu/transport/sites/transport/files/2018-year-multimodality-external-costs-ce-delft-preliminary-results.pdf.
van Essen, H., Schroten, A., Otten, M., Sutter, D., Schreyer, C., Zandonella, R., Maibach, M., Doll, C., 2011. External Costs of Transport in Europe - Update Study for 2008. Tech. Rep. September. CE Delft, Infras, Fraunhofer ISI, Delft. URL. http://ecocalc-test.ecotransit.org/CE_Delft_4215_External_Costs_of_Transport_in_Europe_def.pdf.
Verberght, E., van Hassel, E., 2019. The automated and unmanned inland vessel. J. Phys. Conf. Ser. URL http://iopscience.iop.org/1742-6596/382/1/012014/pdf/1742-6596_382_1_012014.pdf.
Vision++, 2019. Vision++. URL. http://visionplusplus.com.
Wang, L., Groves, P.D., Ziebart, M.K., 2012. Multi-constellation GNSS performance evaluation for urban canyons using large virtual reality city models. J. Navig. 65 (3), 459–476.
Zhang, J., Singh, S., 2017. Low-drift and real-time lidar odometry and mapping. Aut. Robots 41 (2), 401–416.